

Progress in passive daytime radiative cooling: A review from optical mechanism, performance test, and application

Yan Dong^{a,b}, Xinpeng Zhang^a, Lingling Chen^b, Weifeng Meng^b, Cunhai Wang^c, Ziming Cheng^b, Huaxu Liang^{a,d}, Fuqiang Wang^{a,b,*}

^a School of Energy Science and Engineering, Harbin Institute of Technology, 92, West Dazhi Street, Harbin, 150001, PR China

^b School of New Energy, Harbin Institute of Technology at Weihai, 2, West Wenhua Road, Weihai, 264209, PR China

^c School of Energy and Environmental Engineering, University of Science and Technology Beijing, Beijing, 100083, PR China

^d School of Materials Science and Engineering, Nanyang Technological University, Singapore, 639798, Singapore



ARTICLE INFO

Keywords:

Radiative cooling
Solar energy
Radiative transfer
Optical mechanism
Performance test
Expand application
Content

ABSTRACT

By exploiting the 3 K coldness of outer space as heat sink of terrestrial thermal radiation, passive daytime radiative cooling (PDRC) can achieve sub-ambient temperatures without any energy consumption, and thus exhibiting extraordinary application potentials. By pursuing the dual-band (solar and atmosphere window) optical properties to approach ideal 100 %, PDRC can maximize dissipating long wavelength infrared radiation to space and minimize absorbing sunlight simultaneously. PDRC technology can reach 146 W/m^2 theoretical cooling power and up to 120 W/m^2 during application. This article focuses on the fundamental physics mechanism of radiative transfer and natural radiative cooling phenomena. Methodologies of infrared absorption functional group selection, optical band gap selection for solar reflection, photon and phonon enhanced resonance by micro-structure were discussed in detail to give a comprehensive instructing strategy of radiative cooling power improvement. Although PDRC technology can achieve sum-ambient temperature cooling without consuming any energy, its drawbacks such as single function of cooling and high whiteness requirement needed to hinder its large-scale application. This article also outlines the current primary applications of PDRC technology, along with summarizing the challenges and potential opportunities it encounters in practical implementation. This paper aims to provide a comprehensive overview on the fundamental physical mechanisms, methods for enhancing its power output, as well as the current state and future developments of PDRC applications, providing potential guidance for reducing greenhouse gas emissions and energy consumption.

1. Introduction

In the context of global warming and the rapid economic growth—especially in hot, humid areas of developing countries, there is a great demand of pursuing cooling to serve comfortable indoor environments, food storage, and production [1–4]. Conventional refrigeration facilities consume 20 % of the total energy production, contributing to approximately 10 % of global greenhouse gas emissions [5–8]. The escalating world energy consumption for cooling raises concerns about short supply [9–12], exhaustion of energy resources [13–15], and heavy environmental impacts [16–18]. Consequently, there is a severe challenge facing the world to develop an environment-friendly and low-energy-consumption technology with superior cooling capability [19–23].

All substances at a temperature greater than absolute 0 K are composed of moving particles with kinetic energy. The kinetic interactions among moving particles cause charge acceleration and dipole oscillation, which induces the electrodynamic generation of coupled electric and magnetic fields, giving rise to the conversion of heat from the movement of charges in the substances to electromagnetic radiation. Therefore, all substances are in a state of continuous absorption and emission of electromagnetic waves across a broadspectrum of frequencies, while the frequency distribution follows Planck's law and radiant intensity follows the Stefan–Boltzmann law of black-body radiation [24–26].

In the realm of thermodynamics, a process of radiative heat transfer among substances at different temperatures by absorbing and emitting electromagnetic waves with a wide range of frequencies [27–29]. On a planetary scale, when considering radiative energy exchange, the

* Corresponding author. School of Energy Science and Engineering, Harbin Institute of Technology, 92, West Dazhi Street, Harbin, 150001, PR China.
E-mail address: Wangfuqiang@hitwh.edu.cn (F. Wang).

Nomenclatures

C_0	velocity of light in vacuum [m/s]
E_b	(λ , T)
g	asymmetry factor
I	Solar irradiance [W/m^2]
h	Planck constant [J/Hz]
k	Boltzmann's constant [J/K]
N	number of atoms
P_{amb}	atmospheric radiative heating power [W/m^2]
$P_{\text{cond + conv}}$	heat transfer power [W/m^2]
P_{net}	net radiative cooling power [W/m^2]
P_{RC}	radiative cooling power [W/m^2]
P_{sol}	absorbed solar power [W/m^2]
Q_{ext}	extinction efficiency factor
Q_{sca}	scattering efficiency factor

T Temperature [K]

Irradiance of spectral black body radiation [$\text{W}/(\text{m}^2 \mu\text{m})$]	Greek letters
$\epsilon(\lambda)$	Spectral-hemispherical emissivity
λ	Wavelength [μm]
θ	zenith angles [rad]
σ	Stefan–Boltzmann constant [$\text{W}/\text{m}^2\text{K}^4$]

Abbreviations

ATW	atmospheric transmission window
PDRC	passive daytime radiative cooling
PTM	personal thermal management
PE	Polyethylene
PV	photovoltaic
TEG	Thermoelectric generators

earth-atmosphere system operates a mechanically isolated system. This system maintains the energy balance between the energy that earth receives from the sun and the energy the earth loses back into cold outer space (3K) [30–32]. Fig. 1 illustrates the compositional relationship between earth and solar radiation. Of the $\sim 340 \text{ W/m}^2$ of solar radiation received by the earth, an average of $\sim 77 \text{ W/m}^2$ is reflected to the cold outer space by clouds and the atmosphere, an average of $\sim 77 \text{ W/m}^2$ is absorbed by clouds, while about 23 W/m^2 is reflected by the surface albedo, and leaves $\sim 163 \text{ W/m}^2$ of solar radiation input to the earth's energy budget. Despite the tremendous transfers of energy into and from the earth, it keeps a relatively stable surface temperature near 290 K, the earth-atmosphere system uses radiative cooling to emit long wavelength infrared radiation through the earth's atmospheric transmission window (ATW) to balance the absorption of short-wavelength radiation from the Sun [33–36].

In the earth's atmosphere, the ATW mainly falls in the wavelength range of $8\text{--}13 \mu\text{m}$ [37]. Fig. 2 shows the absorption wavelengths of

absorbing molecules in the earth's atmosphere. In the ATW band, the absorptance of long wavelength infrared radiation is close to zero. According to Wien's displacement law, the peak wavelength of terrestrial thermal radiation from earth (about $10 \mu\text{m}$) just in the ATW band. Therefore, exploiting the 3 K coldness of outer space as heat sink of terrestrial thermal radiation is leading to the most promising cooling strategy based on purely passive cooling with zero energy consumption [38–40].

Without the demands of additional energy input, refrigerants or mechanical pumps for maintenance, passive daytime radiative cooling (PDRC) technology can provide a prospective solution to reduce global energy consumption [41,42]. PDRC technology can reflect the majority of incoming solar radiation and simultaneously dissipate heat to outer cold space through the ATW band without any energy consumption [43,44]. By using the 3 K coldness of the space as a heat sink, PDRC technology can achieve sub-ambient temperatures even at peak hours, thus exhibiting remarkable potentiality for passive building cooling, thermal

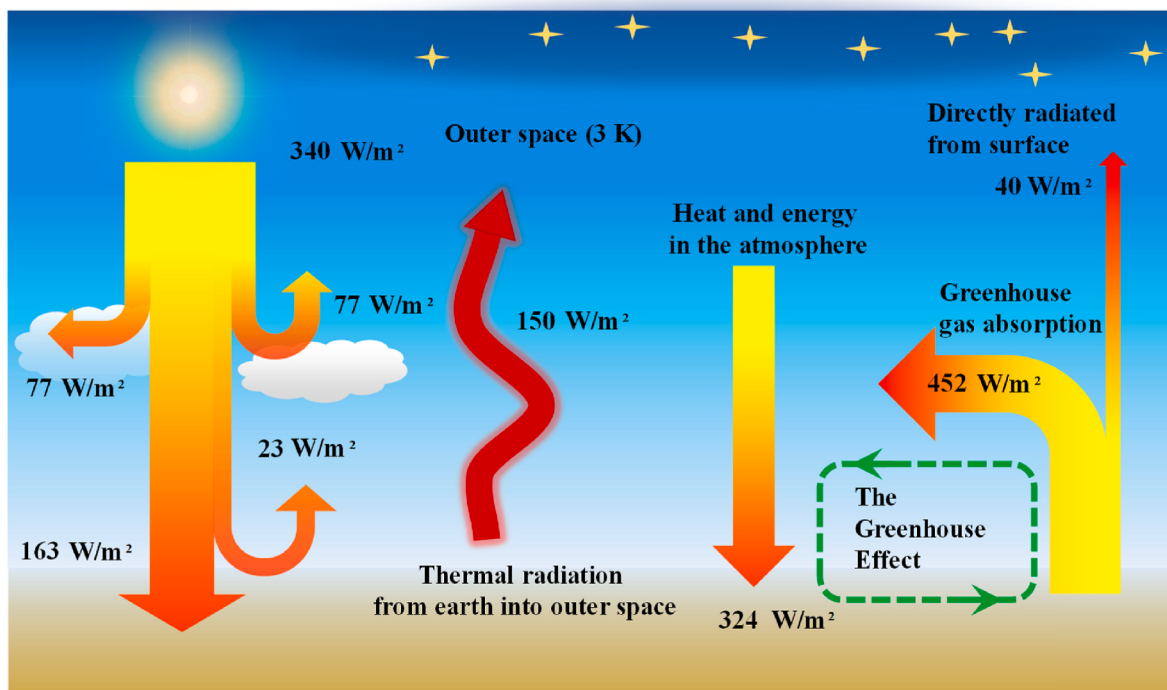


Fig. 1. The important role of radiative cooling in earth's energy budget.

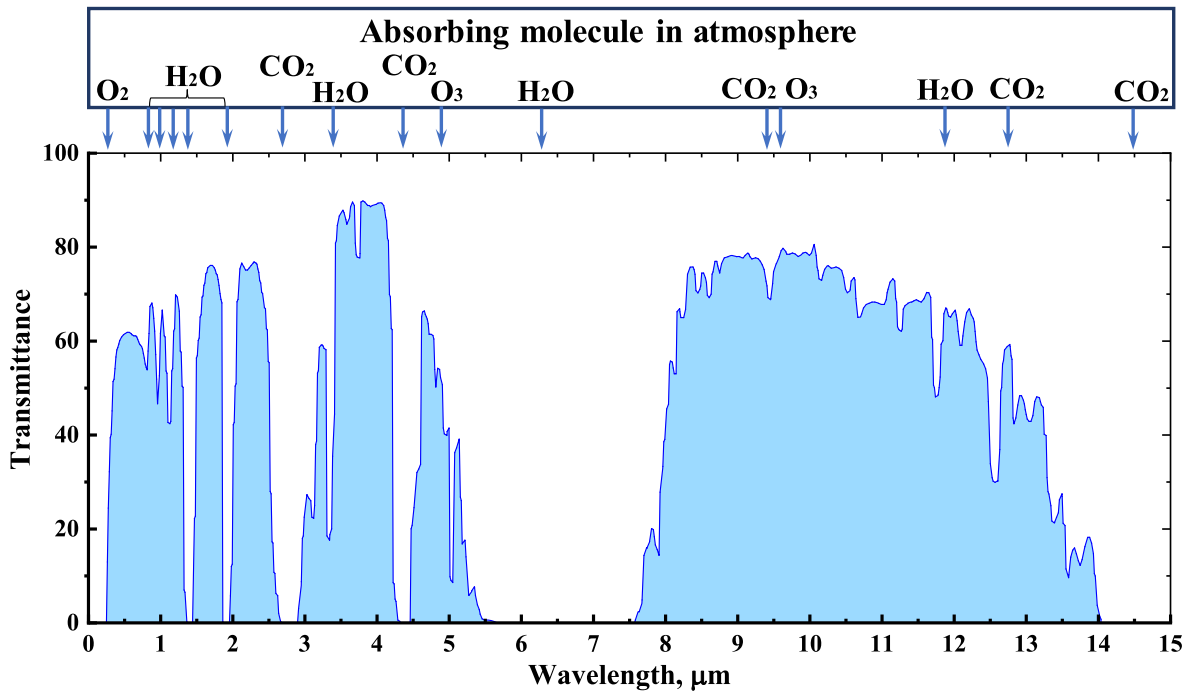


Fig. 2. Absorption wavelengths by CO₂, H₂O, O₂ and O₃ in the earth's atmosphere.

management [45], and local climate change alleviation [46,47]. By integrating high emissivity in the ATW band and high sunlight reflectance, PDRC technology can achieve a theoretical cooling power of 146 W/m² and up to 120 W/m² during application in regions with a dry and hot climate [48,49].

This study offers a comprehensive overview of the fundamental physics mechanism of radiative transfer, the selection of infrared-absorbing functional groups, and the ideal optical properties of PDRC. Given that the preparation and characterization of radiative cooling materials have been extensively summarized in existing literature, this work emphasizes a departure from existing knowledge by focusing on radiative transmission mechanisms in PDRC and material selection methodology for PDRC. It provides comprehensive guiding strategies for enhancing radiative cooling power and expanding application scenarios. Specifically, Section 2 summarizes the physics behind PDRC, encompassing radiation transfer theory and predictions of radiative characteristics. Section 3 delves into radiative cooling phenomena in the natural world. In Section 4, the origin of optical selection characteristics for PDRC materials is introduced. Section 5 details methods like photon and phonon microstructure-enhanced resonance. The application of PDRC is outlined in Section 6. Section 7 provides a summary of this article and outlines the future of PDRC technology for cooling, including its main challenges.

2. Fundamental physics of PDRC

2.1. Fundamental physics of radiative transfer

According to Planck's emissive power law, all substances with a temperature greater than absolute 0 K spontaneously absorb and emit electromagnetic radiation, which is the fundamental physics of radiative cooling. Energy emitted by a substance is in the form of quanta and discontinuous, quantities have different sizes and frequencies of vibration analogous to the wave theory. The energy of each quantum followed the rule $E = h\nu$, where h is the Planck constant and ν is the frequency. High temperature is the origin of high frequency, which can bring out the enhancement of energy in the quantum. Thermal radiation involves the emission of a wide range frequency of electromagnetic

radiation varying on the nature of a surface and the temperature of a substance, which is one of the three basic modes of heat transfer. $I_b(\nu, T)$ can be used to describe the spectral emissive power per unit area (A), per unit solid angle (Ω) for frequency ν at absolute temperature T [50–52]. Assuming that a molecule can emit photons only at different energy levels, Planck predicted the spectral blackbody emissive power distribution, for a black surface surrounded by a transparent media with refractive index n , as

$$I_b(\nu, T) = \frac{2h\nu^3}{C_0^2} \frac{n^2}{\exp(\frac{h\nu}{kT}) - 1} \quad (1)$$

where k is regarded as the Boltzmann's constant with the value of 1.3807×10^{-23} J/K, $h = 6.625 \times 10^{-34}$ J/Hz is known as the Planck constant, C_0 is the velocity of light in vacuum with the value of 2.998×10^8 m/s. Planck's law also reveals that thermal radiation had a maximum intensity at a wavelength that depended on the temperature of the substance. For example, the surface of sun is about 5800 K and is surrounded by vacuum ($n = 1$), its emission peak is close to the middle of the visible wavelength region ($\approx 0.5 \mu\text{m}$). In contrast, the surface of the earth in the vicinity is 290 K–300 K, the earth emitted thermal radiation that is mainly long wavelength infrared and invisible, and the earth's peak emission appeared in the intermediate infrared ($\sim 10 \mu\text{m}$), resulting in infrared cameras and detectors for night "vision". The phenomenon of the peak wavelength shift of black-body radiation in inverse proportion to temperature is referred to as Wien's displacement law, and it is expressed as follows:

$$(n\lambda T)_{\max} = 2898 \mu\text{m}\cdot\text{K} \quad (2)$$

It should be noted that Wien's displacement law is a direct consequence of Planck's emissive power law. The total power emitted by a black body (P_b) per unit area can be predicted by integrating the black body spectral flux over all frequencies and over the solid angles (Ω) corresponding to a hemisphere (h) above the surface [53].

$$P_b = \int_0^\infty d\nu \int_h d\Omega B_\nu \cos(\theta) \quad (3)$$

when the solid angle (Ω) is presented in spherical polar coordinates:

$$d\Omega = \sin(\theta)d\theta d\varphi \quad (4)$$

Therefore,

$$P_b = \int_0^\infty dv \int_0^{\frac{\pi}{2}} d\theta \int_0^{\frac{\pi}{2}} d\varphi B_v(T) \cos(\theta) \sin(\theta) = \sigma T^4 \quad (5)$$

where, σ is the Stefan–Boltzmann constant with the unit of $\text{W}/(\text{m}^2 \cdot \text{K}^4)$, and the value is calculated by:

$$\sigma = \frac{2k^4\pi^5}{15C_0^2h^3} = 5.67 \times 10^{-8} \quad (6)$$

2.2. Ideal optical properties of PDRC

For a radiative cooling cooler, the radiative cooling performance can be increased by increasing the thermal emittance at ATW band to dissipate more heat to the outer cold space and decreasing the solar absorptance to decrease the impact of solar radiation heating [54–56]. Therefore, the optical performance of a PDRC cooler demanded an elaborate design [57,58]. Fig. 3 presents the ideal dual-band spectrum of a PDRC cooler: the average solar reflectance ($\bar{\rho}_{\text{Sol}}$) should be 100 % in the wavelength of 0.25–3 μm to minimize solar heating, while the average emittance in the wavelength of ATW ($\bar{\varepsilon}_{\text{ATW}}$) band should be 100 % to maximize radiating long wavelength infrared energy to the outer cold space. The emittance of a PDRC cooler in other spectral bands ($\lambda = 2.5 \sim 8 \mu\text{m}$ and $\lambda > 13 \mu\text{m}$) should be zero to refrain from the overheating of the atmospheric radiation at a higher temperature [59,60].

The definitions of average solar reflectance and average emittance in the wavelength of ATW are expressed as

$$\bar{\rho}_{\text{Sol}} = 1 - \bar{\alpha}_{\text{Sol}} = \frac{\int_{0.3\mu\text{m}}^{2.5\mu\text{m}} I_{\text{sol}}(\lambda) \rho(\lambda) d\lambda}{\int_{0.3\mu\text{m}}^{2.5\mu\text{m}} I_{\text{sol}}(\lambda) d\lambda} \quad (12)$$

$$\bar{\varepsilon}_{\text{ATW}} = \bar{\alpha}_{\text{ATW}} = \frac{\int_{8\mu\text{m}}^{13\mu\text{m}} I_b(T, \lambda) \varepsilon(\lambda) d\lambda}{\int_{8\mu\text{m}}^{13\mu\text{m}} I_b(T, \lambda) d\lambda} \quad (13)$$

where, $I_{\text{sol}}(\lambda)$ is the ASTM G G173-03 global solar intensity spectrum at AM 1.5, $I_b(T, \lambda)$ is the radiation intensity emitted by a standard blackbody with temperature T , $\rho(\lambda)$ and $\varepsilon(\lambda)$ represent the spectral reflectance and emittance of the PDRC cooler.

During application, the sub-ambient cooling temperature drop by using PDRC techniques generally required the average solar reflectance to be larger than 95 % or at least 90 %, while the average emittance in

the wavelength of ATW should be larger than 90 % [61].

2.3. Theoretical prediction of radiative property

Solving Maxwell's electromagnetic equations provides a direct approach to characterizing the solar reflectivity and infrared emissivity of a PDRC cooler as well as optimizing the substrate material and particle parameters [62,63]. Generally, the finite difference time domain simulation software is adopted to solve the following governing equations of electromagnetic wave propagation:

$$\vec{D}(\omega) = \epsilon_r(\omega) \vec{E}(\omega) \quad (14)$$

$$\frac{\partial \vec{D}}{\partial t} = \frac{1}{\sqrt{\epsilon_0 \mu_0}} (\nabla \times \vec{H}) \quad (15)$$

$$\frac{\partial \vec{H}}{\partial t} = -\frac{1}{\sqrt{\epsilon_0 \mu_0}} (\nabla \times \vec{E}) \quad (16)$$

where D , E , and H represent the electric displacement, electric field, and magnetic field, respectively. $\epsilon_r(\omega)$ is the complex relative dielectric constant, and $\epsilon_r(-\omega)$ is equivalent to the square of refractive index (n^2).

The scalar equations can be expressed as:

$$\frac{\partial D_x}{\partial t} = \frac{1}{\sqrt{\epsilon_0 \mu_0}} \left(\frac{\partial H_z}{\partial y} - \frac{\partial H_y}{\partial z} \right) \quad (17)$$

$$\frac{\partial H_x}{\partial t} = \frac{1}{\sqrt{\epsilon_0 \mu_0}} \left(\frac{\partial E_y}{\partial z} - \frac{\partial E_z}{\partial y} \right) \quad (18)$$

Therefore, utilizing the finite-difference approximations for the scalar equations, it can be expressed as:

$$\begin{aligned} \mathbf{D}_z^{n+\frac{1}{2}} \left(i, j, k + \frac{1}{2} \right) &= \mathbf{D}_z^{n-\frac{1}{2}} \left(i, j, k + \frac{1}{2} \right) \\ &+ \frac{\Delta t}{\Delta x \cdot \sqrt{\epsilon_0 \mu_0}} \left(\mathbf{H}_y^n \left(i + \frac{1}{2}, j, k + \frac{1}{2} \right) - \mathbf{H}_y^n \left(i - \frac{1}{2}, j, k + \frac{1}{2} \right) - \mathbf{H}_x^n \left(i, j + \frac{1}{2}, k + \frac{1}{2} \right) \right. \\ &\quad \left. + \mathbf{H}_x^n \left(i, j - \frac{1}{2}, k + \frac{1}{2} \right) \right) \end{aligned} \quad (19)$$

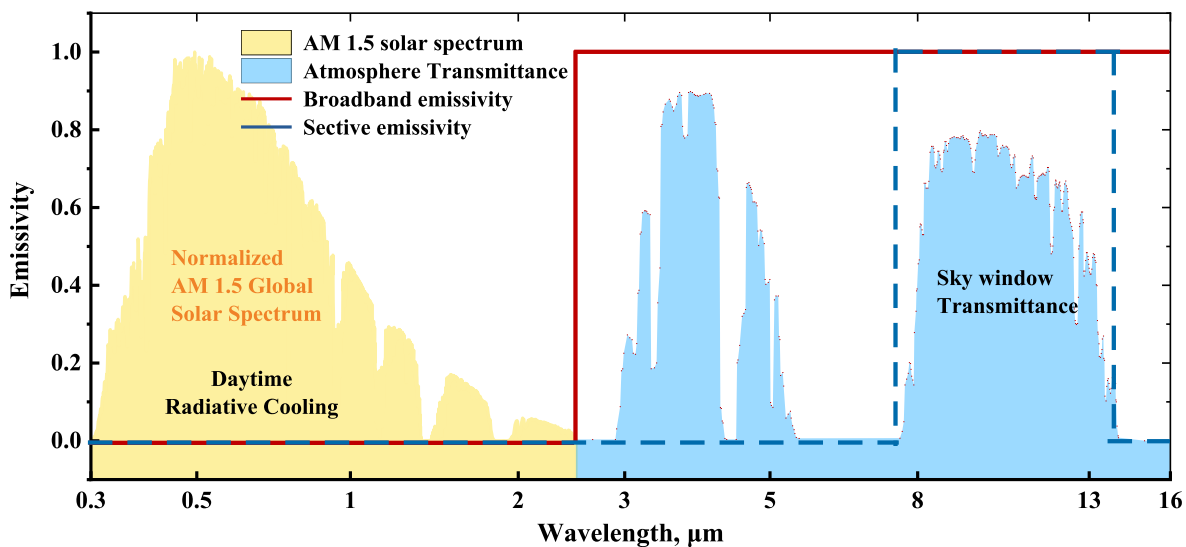


Fig. 3. Ideal dual-band ($\bar{\rho}_{\text{Sol}}$ and $\bar{\varepsilon}_{\text{ATW}}$) spectrum of a PDRC cooler.

$$\begin{aligned} \mathbf{H}_z^{n+1}\left(i+\frac{1}{2}, j+\frac{1}{2}, k\right) &= \mathbf{H}_z^n\left(i+\frac{1}{2}, j+\frac{1}{2}, k\right) \\ -\frac{\Delta t}{\Delta x \cdot \sqrt{\epsilon_0 \mu_0}} &\left(\mathbf{E}_y^{n+\frac{1}{2}}\left(i+1, j+\frac{1}{2}, k\right) - \mathbf{E}_y^{n+\frac{1}{2}}\left(i, j+\frac{1}{2}, k\right) - \mathbf{E}_x^{n+\frac{1}{2}}\left(i+\frac{1}{2}, j+1, k\right) \right. \\ &\left. + \mathbf{E}_x^{n+\frac{1}{2}}\left(i+\frac{1}{2}, j, k\right) \right) \end{aligned} \quad (20)$$

where \mathbf{D}_r and \mathbf{H}_r ($r = x, y, z$) denoted the electric field or flux densities and magnetic field vectors, respectively, and the $\pm 1/2$ terms represented that it was supposed to be located between two steps of E or H values [64,65].

Although solving Maxwell's electromagnetic equations is the straightforward method to obtain and optimize the spectral radiative properties of a PDRC cooler (the coherent scattering of the far and near fields can be considered), it demands too much computational resources and time-consuming. In theory, the PDRC cooler with a mixture of one or more types of particles can be considered as a semitransparent medium containing multi-particle systems having non-uniform size distribution, and the radiative characteristics of a single particle can be obtained through Mie theory to obtain the overall radiative characteristics of the particle system [66–68]. Coupled with the Mie scattering theory and Monte Carlo ray tracing method, Cheng et al. [67] proposed a simplified analysis method with high precision for calculating and optimizing the spectral radiative properties of a PDRC cooler with non-uniform particle size distribution [69–71].

Initially, the Mie scattering theory was adopted to compute the spectral radiative properties of a single particle. For a single particle with a fixed diameter D_i , when it interacted by a bundle of electromagnetic waves with wavelength λ , the extinction efficiency factor Q_{ext} , scattering efficiency factor Q_{sca} , scattering phase function $\Phi(\Theta)$, and asymmetry factor g can be obtained based on electromagnetic wave theory and Mie scattering simplification [72–75]:

$$Q_{ext}(m, \chi) = \frac{2}{\chi^2} \sum_{n=1}^{\infty} (2n+1) Re\{a_n + b_n\} \quad (21)$$

$$Q_{sca}(m, \chi) = \frac{2}{\chi^2} \sum_{n=1}^{\infty} (2n+1) (|a_n|^2 + |b_n|^2) \quad (22)$$

$$Q_{abs}(m, \chi) = Q_{ext}(m, \chi) - Q_{sca}(m, \chi) \quad (23)$$

$$\Phi(\Theta) = 2 \frac{i_1 + i_2}{\chi^2 Q_{sca}} \quad (24)$$

$$g_p = \overline{\cos \Theta} = \frac{1}{4\pi} \int_{4\pi} \Phi_p(\Theta) \cos \Theta d\Omega \quad (25)$$

where m ($m = n-i\kappa$) and χ ($\chi = \frac{\pi D}{\lambda}$) represent the complex index of refraction and size parameter, respectively. n and k are the indexes of refraction and absorption. The spectral complex indexes of refraction of the commonly used materials in PDRC (TiO_2 and SiO_2) in the wavelength range of 0.3–15 μm were illustrated in Fig. 4, which can be easily found in the handbook of optical materials [76].

Then, an algorithm for computing the spectral radiative properties of the multi-particle system was exploited to obtain the spectral radiative properties, embodying the extinction efficiency factor Q_{ext} , scattering efficiency factor Q_{sca} , scattering phase function $\Phi(\Theta)$, and asymmetry factor g . Due to the low volume fraction of particles, the scattering behavior of each particle embedded in the base matrix material of the PDRC cooler can be assumed to be independent of the others [76]. The radiative properties of multi-particle systems having non-uniform size distribution were the same as the properties summed over all the

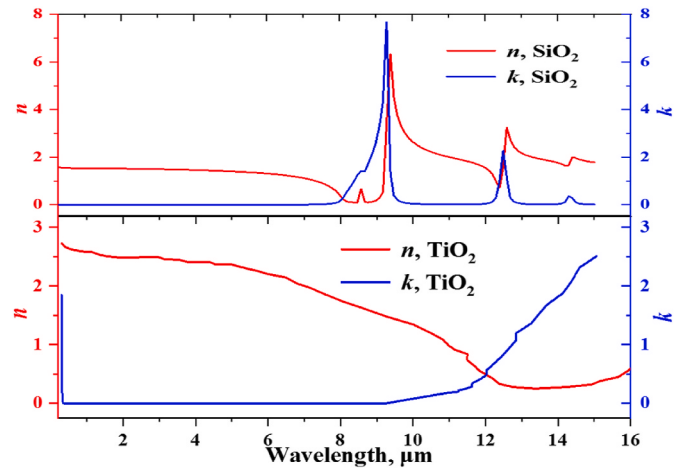


Fig. 4. Complex indexes of refraction and absorption of the SiO_2 and TiO_2 material for wavelengths between 0.3 μm and 15 μm [74].

particles and can be presented as [77,78]:

$$\beta = \sum_{i=1}^n \sum_{j=1}^{n_i} N_{ij} C_{e;ij} = \frac{\pi}{4} \sum_{i=1}^n \sum_{j=1}^{n_i} D_{ij}^2 N_{ij} \frac{Q_{e;ij}}{D_{ij}} = 1.5 \sum_{i=1}^n \sum_{j=1}^{n_i} \frac{Q_{e;ij} f_{v;ij}}{D_{ij}} \quad (26)$$

$$\sigma_s = \sum_{i=1}^n \sum_{j=1}^{n_i} N_{ij} C_{s;ij} = \frac{\pi}{4} \sum_{i=1}^n \sum_{j=1}^{n_i} D_{ij}^2 N_{ij} Q_{s;ij} = 1.5 \sum_{i=1}^n \sum_{j=1}^{n_i} \frac{Q_{s;ij} f_{v;ij}}{D_{ij}} \quad (27)$$

$$\kappa = \beta - \sigma_s \quad (28)$$

It should be noted that the scattering phase function is not identical for all the particles of a multi-particle system with non-uniform size distribution. It can be calculated by integrating the diameter D_{ij} and expressed as:

$$\Phi(\Theta) = \frac{1}{\sigma_s} \sum_{i=1}^n \sum_{j=1}^{n_i} \sigma_{s;ij} \cdot \Phi_{ij}(\Theta) = \frac{1}{\sigma_s} \sum_{i=1}^n \sum_{j=1}^{n_i} \frac{Q_{s;ij} f_{v;ij}}{D_{ij}} \cdot \Phi_{ij}(\Theta) \quad (29)$$

where $\Phi_{ij}(\Theta)$ is the scattering phase function of the i -th type particle with diameter D_{ij} . In the same way, the asymmetry factor g should be revised as:

$$g_{ij} = \frac{1}{2} \int_0^\pi \Phi_{ij}(\Theta) \cos \Theta \sin \Theta d\Theta = \frac{\pi}{2 \cdot n_A} \sum_{h=1}^{n_A} \Phi_{ij}(\Theta_h) \cos \Theta_h \sin \Theta_h \quad (30)$$

where n_A is the number of discrete angle shares, g_{ij} is the asymmetry factor of spherical particles of i -th type and j -th size. By substituting Eq. (30), the asymmetry factor of the multi-particle system possessing non-uniform size distribution can be expressed as:

$$g = \frac{1}{\sigma_s} \sum_{i=1}^n \sum_{j=1}^{n_i} \sigma_{s;ij} g_{ij} \quad (31)$$

Finally, once the radiative properties were acquired, the Monte Carlo ray-tracing method was used to solve the radiative transfer equation of the semitransparent medium containing multi-particle systems [79–81]. The expression of radiative transfer equation is presented in Eq. (32).

$$\frac{dI_\lambda(s)}{ds} = -k_\lambda I_\lambda(s) - \sigma_\lambda I_\lambda(s) + k_\lambda I_{bl}(s) + \frac{\sigma_\lambda}{4\pi} \int_{4\pi} I_\lambda(s, \vec{\Omega}') \Phi_\lambda(\vec{\Omega}', \vec{\Omega}) d\Omega' \quad (32)$$

where I_λ and I_{bl} are the spectral radiative intensity in the direction of $\vec{\Omega}$ along path s and the spectral blackbody intensity, the notation Ω delegated the solid angle. When the average solar reflectivity and emissivity in the ATW band is obtained, the theoretical net radiative cooling power of a PDRC cooler under different operation conditions can be calculated.

The cooling performance of the PDRC cooler is evaluated by net

cooling power, which is controlled by four factors: radiative cooling power (P_{RC}) between the surface of cooler and colder space, absorbed solar power (P_{Sol}), incident atmospheric radiative heating power (P_{Amb}), and heat transfer power ($P_{Cond + Conv}$) with the surrounding media through conduction and convection. Therefore, the net radiative cooling power (P_{net}) of PDRC can be described as [82,83]:

$$P_{net}(T) = P_{RC}(T) - P_{Sol} - P_{Amb}(T_{Amb}) - P_{Cond+Conv} \quad (7)$$

where T is the surface temperature of the substance, T_{Amb} is the ambient temperature.

The radiative cooling power (P_{RC}) of a PDRC cooler can be calculated by:

$$P_{rad}(T) = \int_0^{2\pi} d\Omega \cos \theta \int_0^{\infty} \varepsilon(\lambda) I_B(T, \lambda) d\lambda \quad (8)$$

Based on Kirchhoff's law of thermal radiation, the absorptance $\alpha(\lambda)$ of the PDRC cooler is equal to the emittance $\varepsilon(\lambda)$. The power absorbed by the PDRC cooler due to solar thermal radiation can be calculated as:

$$P_{Sol} = \int_0^{\infty} \varepsilon(\lambda) I_{sol}(\lambda) d\lambda \quad (9)$$

The incident atmospheric radiative heating power (P_{Amb}) absorbed by PDRC cooler can be expressed as:

$$P_{Atm}(T_{Atm}) = \int_0^{2\pi} d\Omega \cos \theta \int_0^{\infty} \varepsilon(\lambda) \varepsilon_{Atm}(\lambda) I_B(T_{Atm}, \lambda) d\lambda \quad (10)$$

The total power loss of all non-radiative heat transfer processes with the surrounding media ($(P_{Cond + Conv})$) is presented as:

$$P_{Cond+Conv} = h_{Cond+Conv}(T - T_{amb}) \quad (11)$$

where $P_{Cond + Conv}$ is the non-radiative heat transfer coefficient, which incorporates the convective heat transfer and conductive heat transfer.

3. Radiative cooling in nature

3.1. Radiative cooling in flora and fauna

Fig. 5 demonstrates the phenomenon of radiative cooling in flora and fauna. The phenomena of passive radiative cooling extensively exist in nature but only happen at clear night since all natural substances absorb more solar radiation energy during the day than the energy dissipated to the cold space by passive radiative cooling. The first study to draft the scientific discussion on the phenomenon of passive radiative cooling in publication was Arago in 1828. As shown in **Fig. 5a**, on a calm and serene night, the top surface temperatures of leaf, grass, cotton, quilt, or any other filamentous materials placed in the open air can be 6–8 K lower than the environmental temperature, because of the effect of passive radiative cooling [84,85].

Living species gradually adapt to the environment during the long evolutionary process [89–93], several faunas in nature have also evolved to use the mechanism of passive radiative cooling to regulate body temperature [94,95]. Saharan silver ant is world-famous as "one of the most heat-resistant animals", as shown in **Fig. 5b**, often traverses midday temperatures around 60–70 °C to capture desert beetle or scavenge corpses of heat-stricken animals, while its body temperature measured as "operative environmental temperatures" is in the range of 48–51 °C. Norman et al. [96] revealed that the Saharan silver ant could regulate electromagnetic waves over an enormously wide region of the electromagnetic spectrum (from the solar spectrum to the ATW band) and that various physical mechanisms were exploited in different wavelength regions to attain a momentous biological function: 1) the hair with unique shape had ultrahigh reflection in the visible and near-infrared wavelength band to minimize solar heating, 2) and the hair also had ultrahigh emission in the long wavelength infrared band to dissipate the heat generated by the hot body through passive radiative cooling [97].

Darkling beetles of the Namib Desert [98], as shown in **Fig. 5c**, living in hot and arid regions and have evolved to be extremely tolerance to

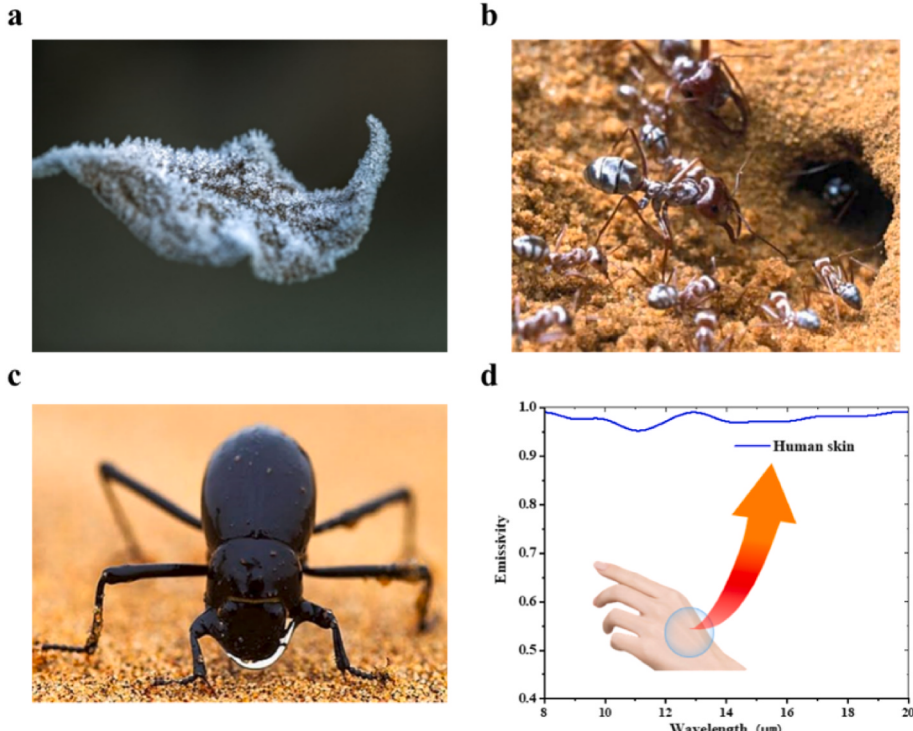


Fig. 5. Radiative cooling phenomena in flora and fauna: (a) leaf covered with ice crystals [86]. (b) silver ants live in Sahara desert [87]. (c) Darkling beetles condense dew from air [88]. (d) Human skin with high ATW emissivity.

such harsh water-limited ecosystems. The black body with nano-structures of Namib beetles has high emission in the ATW band, and can cool its body temperature below the air temperature. The wings and certain body positions of Namib beetles with permeable integuments can produce dew from condensing humid air [98].

Human is warm-blooded animal and has been evolved to adapt to various complex environments. As shown in Fig. 5d, human skin can be approximated as a perfect infrared emitter, with an infrared emissivity of 97 % in the ATW band, which keeps the record of emissivity in medical thermal imaging. The following three biological tissue structures induce the human skin as a blackbody with superior infrared emissivity: 1) Massive small cavities on the epidermis layer. Each cavity can be approximated as a blackbody, which emits long wavelength infrared energy efficiently. 2) Wrinkle micro-structure on the epidermis layer formed by keratinized [99–101] stratified squamous epithelium. Electromagnetic theory analysis shows that the exquisitely designed wrinkle micro-structure can further increase the average infrared emissivity by 4.5 % compared to the planar surface [102]. 3) Three-dimensional staggered arranged collagen fibers with captured aqueous hyaluronic acid in the dermis layer.

3.2. Radiation fog

Fog is a visible aerosol formed by small water droplets or ice crystals suspended in the air at or close to the ground surface, formed when the temperature difference between air and dew point is less than 2.5 °C [103,104]. Radiation fog, a common type of fog, usually generated in the winter nighttime. As shown in Fig. 6, radiation fog generate at or close to the surface, intensification since the air continues to be chilled down [105]. The following two conditions are benefit to form radiation fog: 1) a shallow surface layer of relatively moist air below a dry layer and clear skies, and 2) small surface winds since the wind would destroy its formation [106,107]. Radiation fog forms at night and is generally patchy, prone to stopover in one place, and disappears soon after sunrise as the ground warms. Radiation fog may sustain for a whole day in the winter months, especially in high elevation areas since the sunlight has little impact on heating the ground. In southwest China, it is observed that radiation fog can be beneficial to the production of crop, since radiation fog can absorb part of the high-intensity solar radiation during the morning shours and thus alleviate the photodamage inflicted by chilling [108]. Recent theoretical research indicates that radiation fog can greatly influence the radiative energy budget in the Arctic, since the fog can arise up to forty percent of the time in Arctic winter and its radiative cooling energy can reach 60 W/m² [109].

3.3. Radiative cooling in planets for energy exchange

The earth with a typical temperature of 290 K applies radiative cooling to emit long-wavelength infrared energy to balance the absorption of short-wavelength sunlight radiation. In space, radiative

transfer is one of the few ways for stars to exchange energy. Take a white dwarf star as an example, it has a high temperature at the initial stage of formation. Without any energy generated by fusion or gravitational contraction, nor any heating from the solar wind, a white dwarf will gradually drop in temperature as it dissipates heat to space by radiative cooling. Therefore, the age of a white dwarf is a function of temperature. By measuring the surface temperature, the age of a white dwarf star can be predicted. Before the development of radiometric age-dating of meteorite technology, the calculation of radiative cooling power was also used to predict the age of earth, which was initially put forward by Baron Kelvin in 1862. Baron Kelvin hypothesized the earth as a completely molten object and calculated the elapsed time it needed to consume for the near-surface temperature gradient to diminish to its current value.

4. Material selection methodology for PDRC

A profound understanding of the origin of the optical selection property of a PDRC cooler, especially the intrinsic of infrared radiation and solar reflection, can give theoretical guidance to design PDRC and base material selection.

4.1. Intrinsic of infrared radiation

Quantum theory research indicates that the essence of the infrared wavelength absorption and emission is attributed to the interaction between molecular dipole changes of rotational-vibrational movements and the light oscillatory electric field [111–113].

Infrared radiation can excite vibrational modes in a molecule through a variation in the dipole moment, forming a beneficial wavelength range for research of such energy conditions for molecules of the proper symmetry. Fig. 7 illustrates the electromagnetic spectrum with typical temperature. Theoretically, matter emits infrared radiation across the full spectrum of wavelengths. Infrared radiation is usually divided into three regions according to the relative molecular or electromagnetic wave properties: near infrared radiation (nearest the visible spectrum) with a wavelength range of 760 nm–2500 nm; middle infrared radiation with a wavelength range of 2.5 μm–25 μm; and far infrared radiation with the wavelength range of 25 μm–1000 μm. The near infrared radiation with higher frequency and energy can excite the overtone or combination modes of molecular vibrations. The middle infrared radiation is usually adopted to research the fundamental vibrations and related rotational-vibrational structure. While far infrared radiation with lower frequency and energy can be adopted to explore rotational spectroscopy and low frequency vibrations.

The infrared radiation is emitted or absorbed by a PDRC cooler when the frequency of absorbed radiation is consistent with the vibrational frequency, inducing a resonance phenomenon. According to the harmonic approximation and Born–Oppenheimer approximation, the resonant frequency is related to the normal modes of vibration

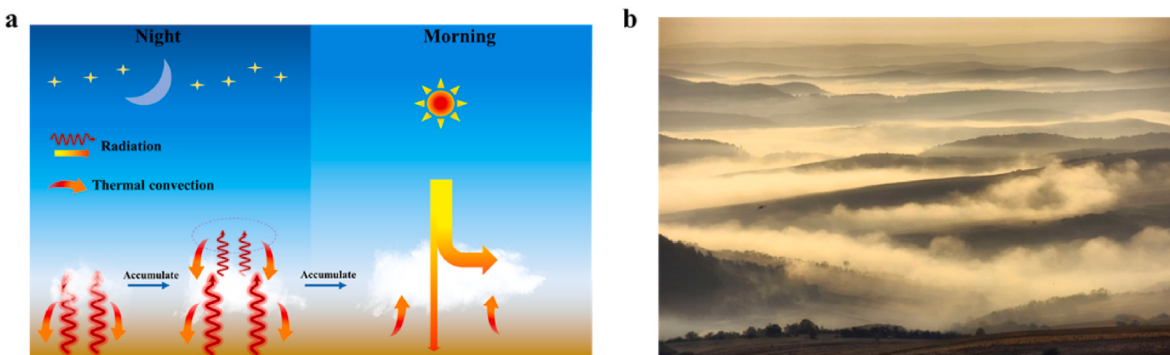


Fig. 6. Principle (a) and photograph [110] (b) of radiation fog formation.

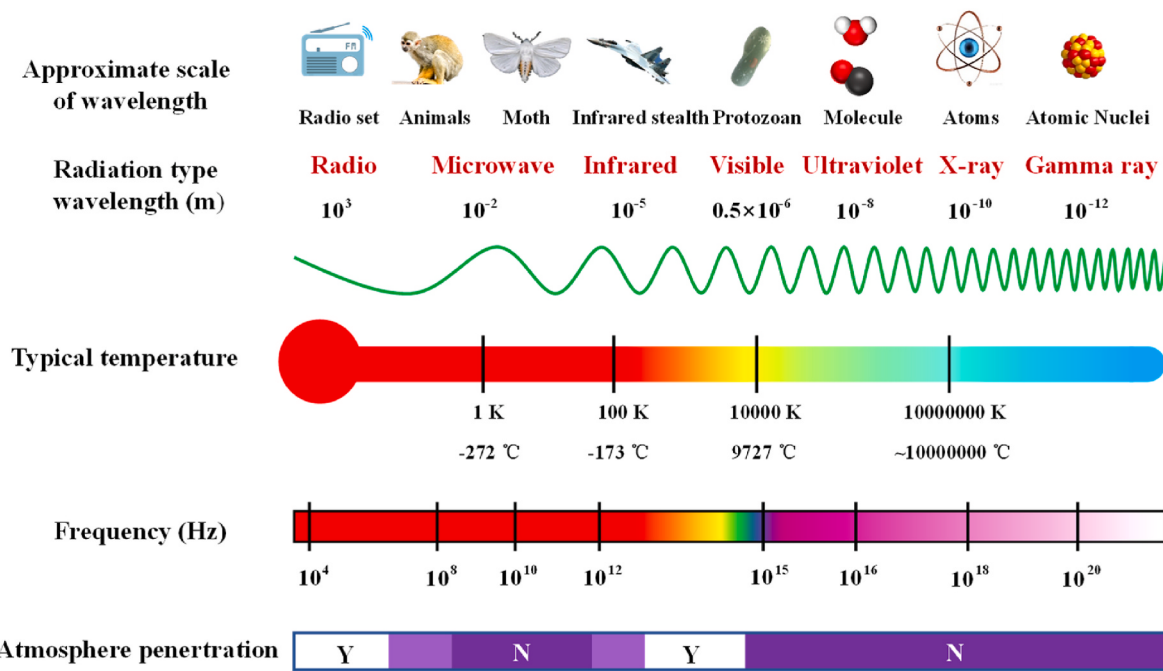


Fig. 7. Electromagnetic spectrum with typical temperature.

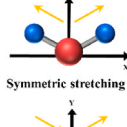
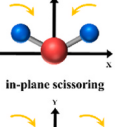
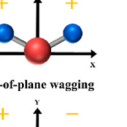
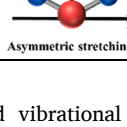
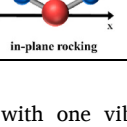
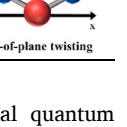
corresponding to the molecular electronic ground state potential energy surface. Functional group (i.e.: N–H, C–F, C=C, R₂C=CR₂, R₃SiOR) is a group of atoms in a molecule that induces the distinctive physical or chemical properties of the molecule. Its resonant frequency is determined by the bond strength and mass of the atoms at each end of bond. Therefore, the vibration frequency of a functional group is highly related to a specific normal mode of movement and a specific bond characteristic.

As shown in Table 1, a molecule with several functional groups can vibrate in various modes [114], and the degrees of vibrational modes are determined by both the number of atoms (N) and geometrical structure of molecules: a molecule with N number of atoms and geometrically linear structure (i.e.: CO₂, XeF₂, BeF₂) has three degrees of translational freedom and two degrees of rotational freedom, $3N - 5$ numbers of vibrational modes and total $3N$ number degrees of total freedom. For a molecule with geometrically non-linear structure (i.e.: SO₂, H₂O, BF₃), it has three degrees of translational freedom and three degrees of rotational freedom, $3N - 6$ numbers of vibrational modes, and total $3N$ number degrees of total freedom.

The methylene functional group (–CH₂–), a part of a molecule connected to the rest of the molecule by two single bonds, is widely found in organic compound of PDRC cooler base materials (i.e. PVDF and PMMA) and has the six fundamental types of vibrational modes, including (as shown in Table 2): two stretching vibrations: symmetric in radial direction and antisymmetric in radial direction; and four bending modes: scissoring in latitudinal direction, rocking in latitudinal direction, wagging in longitudinal direction and twisting in longitudinal direction.

The basic or principal infrared wave band absorption occurs when the functional group of a molecule is distorted, the normal mode is excited from the ground state with zero vibrational quantum number to

Table 2
Vibration modes of functional groups in polymers.

Direction Symmetry	Radial	Latitudinal	Longitudinal
Symmetric	 Symmetric stretching	 in-plane scissoring	 out-of-plane wagging
Antisymmetric	 Asymmetric stretching	 in-plane rocking	 out-of-plane twisting

the initial excited vibrational state with one vibrational quantum number. Occasionally, the overtone band happens at almost twofold the energy of the fundamental band for the same normal mode, due to the absorption of a photon giving rise to a direct transition from the ground state to the second excited vibrational state. Fermi resonance often arises between fundamental and overtone excitations when two excitation modes are similar in energy, it can induce an unanticipated change in energy modes and intensity of the bands [115].

4.2. Selection of infrared absorption functional group

When infrared light strikes a material, the absorption happens if the frequency of the incident infrared light coincides with the vibrational frequency of a bond or collection of bonds. Infrared light spectroscopy is equivalent to transitions between the vibrational energy levels of a molecule, referring to the stretching or bending of bonds. Infrared transition yields as a result of the interaction of the oscillating electric vector of the infrared light with the oscillating dipole moment of the molecule (owing to the molecular vibration). The principle of selecting for infrared transitions - which needs to be followed when infrared absorption is to occur for a specific vibration - elaborates that the molecule needs to possess a dipole moment and there needs to be a variation in the molecular dipole moment during the vibration, i.e. the dipole moment needs to be different at the extremes of the vibration. Comparing two

Table 1
Degrees of vibrational modes.

Type of degrees of freedom	Linear	Non-linear
Translational	3	3
Rotational	2	3
Vibrational	$3N - 5$	$3N - 6$
Total	$3N$	$3N$

bonded atoms two vibrating objects interlinked by a spring (a simple harmonic oscillator), the wavenumber of the vibration for the system can be expressed by Hooke's law:

$$\nu = \frac{1}{2\pi} \sqrt{\frac{k}{\mu}} \text{ or } \bar{\nu} = \frac{1}{2\pi c} \sqrt{\frac{k}{\mu}} \quad (33)$$

where k delegates the force constant of the bond (N/m) - stronger bond has a larger value of k ; $\bar{\nu}$ delegates the wavenumber (cm^{-1}); ν denotes the frequency (Hz); c delegates the speed of light ($3 \times 10^8 \text{ m/s}$); and μ denotes the reduced mass with the unit of kg:

$$\mu = \frac{m_1 \times m_2}{m_1 + m_2} \quad (34)$$

where m_1 equals the product of relative atomic mass (M_1) and atomic mass unit, and the symbol m_2 equals the product of relative atomic mass (M_2) and the atomic mass unit with the value of $1.66 \times 10^{-27} \text{ kg}$.

For a PDRC cooler, the region of interest for infrared spectroscopy is in the wavelength range of $2.5\text{--}15 \mu\text{m}$, which is also the most diagnostic region for vibrations occurrence. For a material with ultrahigh purity and a small amount of infrared light active bonds, few vibration modes are excited and a small quantity of absorption spectra is observed on infrared spectroscopy. Some of these bands can only give credit to vibrations of the whole molecular skeleton; these bands happen between 1500 and 1000 cm^{-1} and are characteristic of the molecule. Herein, this wavenumber range is entitled the "fingerprint region", it is similar to the fingerprint which is one-of-a-kind of a human body, the modality of infrared bands in this wavenumber range is sole to a specific molecule. Some of the infrared absorption bands can give the credit to the vibration of individual bonds, and these bands are the most diagnostically useful because it can be a favor to identify the functional groups that exist in the molecule.

For PDRC cooler base materials (i.e. PVDF and PMMA), it had multiple types of functional groups with diverse vibration modes and induced a substantial number of infrared absorption/emission peaks in PDRC cooler. Fig. 8 shows the major band assignments for infrared spectra of common chemical bonds. Typical functional groups bring about distinctive molecular bonds both in terms of infrared light absorption peaks and frequencies (or wave numbers), which are mainly

influenced by the following three factors [116–119]:

- 1) Whether there is H in a functional group. The atomic mass of H is the smallest, and the reduced mass of the chemical bond connected with H (μ) is very small. According to Lambert Beer's law ($\sigma = (1/2\pi c)[(k/\mu)]^{1/2}$), such chemical bonds generally located in the high wavenumber region.
- 2) Chemical bond type. The common functional groups are located in the wavelength range of $4000\text{--}600 \text{ cm}^{-1}$. According to the vibration form of different chemical bond types, it can be divided into four regions (it should be noted that different references may have small differences on the wavenumber region division).
 - $4000\text{--}2500 \text{ cm}^{-1}$. Vibrations of single bonds to H, which is titled as X-H stretching vibration region (C-H, O-H, N-H, and S-H).
 - $2500\text{--}2000 \text{ cm}^{-1}$. Vibrations of triple and cumulative bonds, which are titled as triple bond (C≡C, C≡N) and cumulative double bond stretching vibration region (N≡C=N, N≡C=S, N≡C=O).
 - $2000\text{--}1500 \text{ cm}^{-1}$. Vibrations of C=X, which is titled as double bond expansion vibration region (C=N, C=C, C=O).
 - $1500\text{--}600 \text{ cm}^{-1}$. Unsaturated C-H bending and X-Y expansion and vibration regions, which is titled as fingerprint region (C-Cl, C-F).
- 3) Chemical bond force constant. Generally, the bond force constant (k) follows the relationship of $k_{\text{triple}} > k_{\text{double}} > k_{\text{single}}$. On the basis of Lambert Beer's law, the larger the chemical bond force constant is, the higher wave number region is located.

PMMA, PVDF, and PLA polymers have several functional groups which may have C=O ($1825\text{--}1725 \text{ cm}^{-1}$), -CH3 (1454.49 cm^{-1}), -CH (1382 to 1300 cm^{-1}), C-O($1042\text{--}1267 \text{ cm}^{-1}$), and C-C (867.67 cm^{-1}), C-O-C ($1260\text{--}1110 \text{ cm}^{-1}$) or C-OH ($1239\text{--}1030 \text{ cm}^{-1}$) bonds vibrations, and these chemical bond vibrations can exhibit strong infrared absorption in the ATW band. Besides, PMMA, PVDF, and PLA polymers have negligible extinction coefficients in the solar wavelengths intrinsically. Therefore, PMMA, PVDF, and PLA polymers had ideal intrinsic dual-band optical properties to enable high performance PDRC applications, which are often used as the matrix for PDRC [120–122].

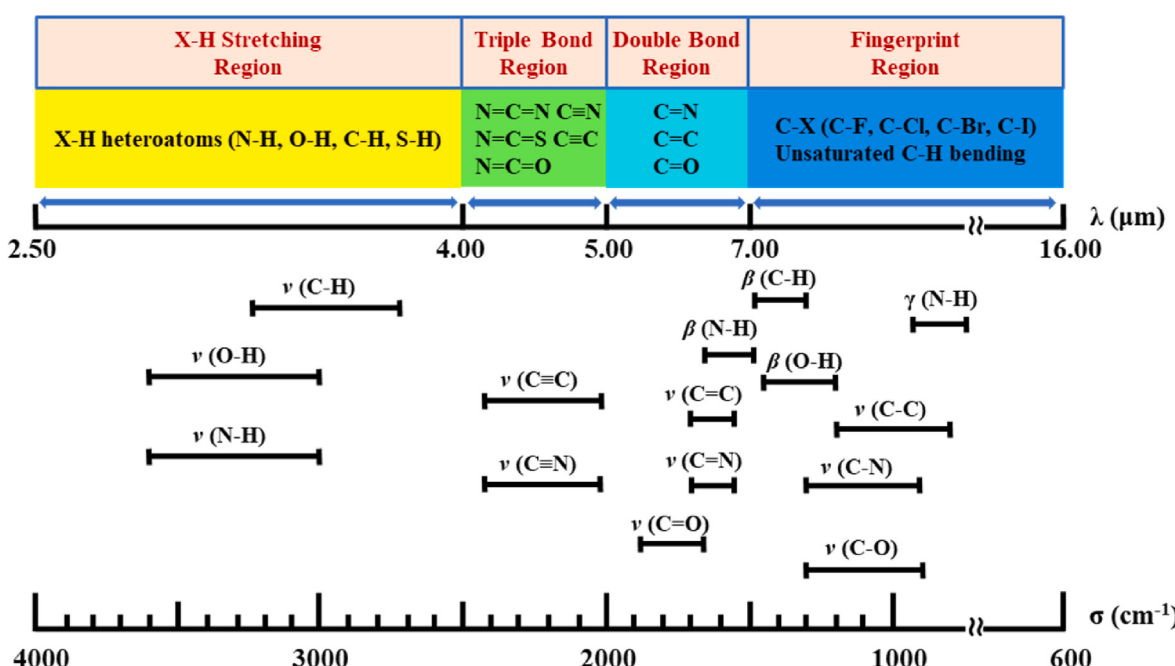


Fig. 8. Major band assignments for infrared spectra of common chemical bonds.

4.3. Optical band gap selection for solar reflection

When an electromagnetic wave propagates from a substance of a specific refractive index into another substance with a different refractive index, the direction of a wavefront at an interface between two different substances is altered and the wavefront of an electromagnetic wave turns back to the medium from which the electromagnetic wave emitted, the phenomenon of light reflection is generated [123–125]. The physics mechanism of reflection can be explained by classical electrodynamics theory as: when a bundle of electromagnetic wave strikes on a medium, it can incur small oscillations of polarization in the individual atoms (or oscillation of electrons, in metals), and leads every particle to radiate a small secondary electromagnetic wave in total directions, analogous to a dipole antenna. Based on the Huygens–Fresnel principle, all these waves overly together form specular reflection and refraction. The refracted electromagnetic wave in the dielectric medium is the combination of the forward radiation of the electrons and the incident electromagnetic wave. The reflected electromagnetic wave is the combination of the backward radiation of all the electrons.

The average radiative cooling power of a PDRC cooler in a cloudless is only 60–120 W/m², while the received sunlight heating is up to 1000 W/m² which is about tenfold magnitude higher than the radiative cooling power [126,127]. To obtain a net radiative heat loss with superior sub-ambient cooling performance under direct solar heating, it is necessary to reach high solar reflectivity and emissivity in the ATW band simultaneously. Duo et al. [128] conducted a theoretical analysis comparison on the temperature drop of PDRC between the ideal selective radiator and non-selective radiator. Duo et al. [128] regarded that a non-selective thermal radiator with absorption/emission beyond the atmospheric transparency window would absorb downward thermal radiation from the atmosphere and consequently weaken the cooling performance. In the case of preventing the re-absorbing of atmospheric radiation, it is also necessary to have high reflectivity in the wavelength of 2.5–8 μm.

The meticulous selection of material with a low-refractive index, including pigments and polymer binder, is the fundamental guarantee of high reflection in a PDRC cooler to decrease the solar absorption (increase solar reflection). The optical band gap fixes on which part of the solar radiation spectrum a dielectric medium absorbs. The photons with energy lower than the optical band gap will be reflected or transmitted, while the photons can only be reflected for opaque medium. A wide optical band gap usually corresponds to a small refractive index and a blue-shifted absorption edge wavelength. The relationship between band gap and absorption edge wavelength is expressed as:

$$\lambda_{\text{Edge}} = 1240/E_g \quad (35)$$

Table 3 shows the optical parameters of common dielectric particles. Existing dielectric particles those are widely used in PDRC, such as Al₂O₃ and BaSO₄, have a very wide optical band gap (7.0 eV and 6.0 eV) and low refractive index (1.78 and 1.64 at 500 nm) with the absorption edge wavelength of 177 nm, 207 nm, respectively. Al₂O₃ and BaSO₄ particles have the intrinsic characteristics of optical phonon resonances or vibrational modes in the thermal infrared wavelengths, which leads them extraordinarily appropriate for passive radiative cooling. However, the industry preferred to use cost-effective TiO₂ particles as a white

pigment, because the high refractive index contrast between TiO₂ nanoparticles ($n > 2.5$) and polymer matrix (≈ 1.5) enables TiO₂ to scatter sunlight more effectively than other white pigments of the same amount. Due to the narrow band gap of TiO₂ (3.2 eV) with higher absorption edge wavelength ($\lambda_{\text{Edge}} = 387.5$ nm), the mere usage of TiO₂ can cause considerable absorption in the UV band, which absorbs about 7 % solar energy and limits the solar reflectivity of TiO₂-based coatings to be smaller than 93 % [129–132]. To resolve this problem, Dong et al. [133] put forward the idea of introducing making layer in PDRC coating: the TiO₂ micro-particles is used in the bottom layer as a masking layer to provide hading power and Al₂O₃ micro-particles that have wide optical band gaps are encapsulated in the reflecting layer to further increase the solar reflection.

5. Photon and phonon enhanced resonance by micro-structure

To increase the sunlight reflection of a PDRC cooler, the deflection angle of the scattered electromagnetic wave should be completely backscattered theoretically, since this can decrease the amounts of scattering events needed to reverse the incoming electromagnetic wave [134–136]. The strict demand for high solar reflectivity can be attained through backing silver coating [137–139] or by multiple scattering using low-loss porous nano/microstructures [140–143]. Together with elaborately designed or selected base material, nano/microstructures such as: micro- or nano dielectric particles [144–146], photonic crystals [147–150], porous [151–154], multilayer film [155–158], and plasmonic structures [159–161], is usually adopted to regulate the radiative properties of backscatter sunlight and phonon-enhanced Fröhlich resonances, which can further increase the solar reflectivity and ATW emissivity.

5.1. Multiple-enhanced Mie and phonon resonances by micro-particles

Micro- or nano dielectric particles with optimized parameters can exploit the conjoint effects of multiple Mie resonances and generate the scattering peaks required to span the whole wavelength of sunlight with high reflectivity [162–164]. The material type, size, and shape of the particles have critical impact on the direction in which the incoming electromagnetic wave is scattered [165–167], which is generally evaluated by asymmetry factor (g) and ideal backward scattering with smallest g . In principle, the optical band gap of micro- or nano dielectric particles needs to be higher than the energy of solar photons (0.49–4.13 eV) to prevent absorption of solar radiation, while the size of micro- or nano dielectric particles should be consistent with the wavelength of sunlight in the base material. Taking the particle size as an example, on the basis of Mie scattering theory, the scattering peak generally has a redshift with the increased particle size. Therefore, the increase of average radius of randomly distributed functional particles in a PDRC cooler could induce the redshift of solar reflectivity [168–170].

Yang et al. [171] proposed to use the phonon-enhanced Fröhlich resonances of the microspheres to enhance the emissivity across the entire ATW wavelength. SiO₂ micro-particles with an average radius of 4 μm can effectively excite the high-order Fröhlich resonances at the extinction peak including both electric and magnetic modes. The PDRC film coated with silver layer can reflect nearly 96 % of the incoming sunlight and achieve an infrared emissivity of larger than 93 % in the ATW wavelength. Huang et al. [172] proposed to use the mixture of titanium dioxide particle and carbon black particle to achieve a double function of high sunlight reflection and high infrared emission in the ATW band for a PDRC coating. The impacts of the particle radius and particle size distribution on radiative properties of the PDRC coating was investigated based on the Mie scattering theory and solving the radiative transfer equation. The numerical analysis indicated that the PDRC coating with particle radius of 0.2 μm had the best optical performance. Theoretically, both the solar reflectivity and emissivity in the ATW band can be higher than 90 %, while the net radiative cooling power can reach

Table 3
Optical parameters of common dielectric particles.

Particle type	Optical band gap	Refractive index	Absorption edge wavelength
Solar photons	0.49–4.13 eV	/	/
BaSO ₄	7.0 eV	1.64	177 nm
Al ₂ O ₃	6.0 eV	1.78	207 nm
TiO ₂	3.2 eV	2.56	387.5 nm

100 W/m² [173–176]. Due to the scatterers with high refractive indices, Zeng et al. [120] proposed to embed TiO₂ microparticles with size distributions between 200 and 1600 nm in composite woven textile to utilize the aggregative effect of multiple Mie resonances. The prepared woven based PDRC metafabrics can realize a solar reflectance of 92.4 % and infrared emissivity of 94.5 % in the ATW band.

To decrease the manufacturing cost for large scale application, Dong et al. [83] adopted using the spectral band complementarity idea to achieve super-high solar reflectivity and good radiative cooling performance. Three types of micro dielectric particles (BaSO₄, CaCO₃, and SiO₂) with particle size commensurate with the wavelength of sunlight were well chosen and embedded in acrylic acid matrix for optical regulation in different wavelengths by using the spectral band complementarity methodology to achieve ultrahigh solar reflectivity. The scattering phase function, electric field, scattering and absorption efficiency variation with particle size for different particles obtained by solving the Maxwell's equations are presented in Fig. 9. The solar reflectivity of the PDRC coating can reach 97.6%, while the theoretical net radiative cooling power can reach 119.3 W/m² and 94.3 W/m² at nighttime and daytime [83].

Several non-sphere type particles were also put forward to increase the backward scattering effect of sunlight and minimize solar absorption for PDRC technology. A hollow dielectric particle was initially introduced by Chen et al. [168] to enhance the amount of interfaces between the air and dielectric, which can in turn increase the net solar reflectivity. The numerical analysis indicated that the PDRC cooler with hollow dielectric particles can obtain a net cooling power of 77 W/m² at ambient temperature of 25 °C, which was 64 % larger than that of the PDRC cooler with sphere type particle. Bao et al. [129] proposed to use h-BN as the particle material for PDRC due to the wide band gap (5.96 eV), large refractive index (2.2 at 500 nm), and high thermal conductivity (over 400 Wm⁻¹K⁻¹). Electromagnetic theory analysis showed

that the distinctive nanoplate type h-BN particle had an isotropic scattering with a larger angle-weighted scattering coefficient, which can achieve a much larger backward scattering efficiency. The solar reflectance of the prepared PDRC film can reach 0.98, while the infrared emissivity in the ATW band is only 0.90. Over two days outdoor test, the PDRC film with nanoplate type h-BN can reach an average sub-ambient cooling temperature of 7.3 °C.

5.2. Photon and photon-enhanced resonance by bio-inspired micro-surface

Currently, PDRC materials with periodic photonic structures, such as metallic photonic crystals and plasmonic nanostructures with regularity, exhibit highly selective optical emissions in the infrared wavelength band [174,175]. However, surface microstructures with periodicity and regularity adopted have weaknesses such as intricate design requirements, elevated manufacturing expenses, and intricate procedural intricacies. Several biological creatures of nature have exhibited excellent photonic micro-structures for radiative heat dissipation without the need for regularity, such as human skin with random distributed wrinkle microstructure [176–179], white beetle with shell/hollow micro-cylinder structures [180], silvery butterfly with irregular scales, Sahara silver ants with triangular shaped hairs [96], and longicorn beetles with dual-scale fluffs, had demonstrated to selectively emit the infrared radiation in ATW band through surface phonon resonance. Mimicking biological photonic structures for radiative property regulation in the visible to infrared wavelength denotes an advanced technical path of fabricating a PDRC cooler with excellent characteristics of anisotropy, ultra-broad band, spectrally selective, and polarization sensitive emission.

The infrared emissivity of human skin in the ATW band can reach 0.97, which is a near-perfect infrared emitter and holds the highest on

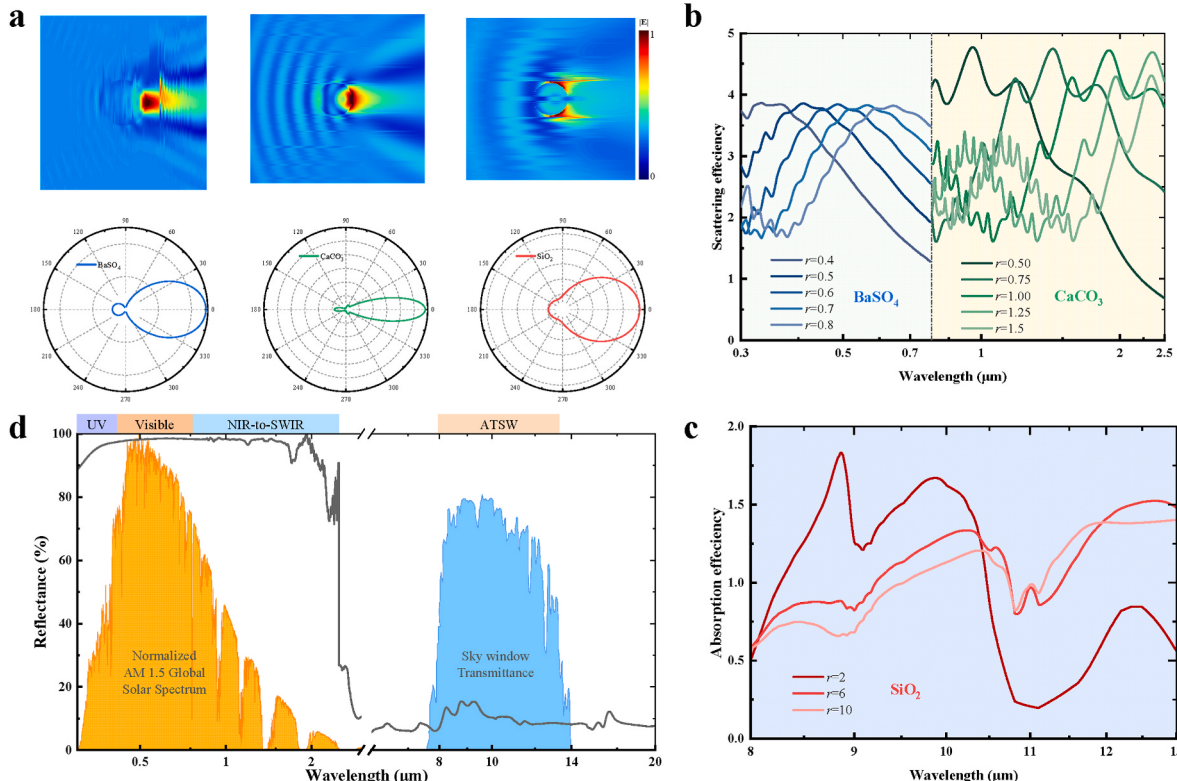


Fig. 9. Spectral band complementarity to achieve high solar reflectivity and good radiative cooling performance [84]. (a) Scattering phase function and electric field of the PDRC cooler with different materials. (b) The scattering efficiency for particles of different sizes. (c) The absorption efficiencies for particles of different sizes. (d) The reflectance of the PDRC coating in AM1.5 solar spectrum and ATSW spectrum of the PDRC cooler. Figures reproduced with permission from (a-d) Dong et al., *Renew. Energy* 292, 606–616 (2022). Copyright 2022 Elsevier.

record for infrared emissivity in medical thermal imaging. Inspired by the optical mechanism of wrinkle structure of human skin, the methodology of employing bioinspired wrinkle micro structure coupled with elaborately selected micro-particles to realize the efficient spectral radiative property oriented design of both the solar band and ATW band was put forward by Wang et al. [49,102]. During solvent evaporation, when the stress on the surface exceeds the critical value of the surface stability, it causes surface instability and triggers the formation of wrinkles. To control the size of natural wrinkle height precisely, Wang et al. have conducted several pre-tests in the development process of the Bio-RC coating, and summed up the preparation experiences. The research results are shown in Fig. 10b, for bio-skin inspired PDRC coating with a thickness of 100 μm , the average solar reflectivity (\bar{R}_{solar}) can achieve ~95 %, and the average infrared emissivity ($\bar{\epsilon}_{\text{atm}}$) in the ATW band can achieve ~96 %, which are 1 % and 3 % higher than the planar coating of the identical thickness, respectively. Feng et al. [177] designed and prepared a bio-skin inspired 3D porous nano-laminated PDRC cooler using the surface droplet-spattering method. As shown in Fig. 10c and d, compared to planner surface, the micro-wrinkled surface and dense nano-layer can increase the solar reflectivity and infrared emissivity in the ATW band by 6.0 % and 7.9 %, respectively.

Research from Columbia University revealed that silver ants had evolved to regulate the wide spectrum of electromagnetic waves (from visible to infrared light) and various physical mechanisms were adopted in different wavelength bands to achieve an expected biological function [96]. Intensive hairs with a special triangle shape were found on the top and bilateral sides of the silver ant's body. Fig. 11a and b shows the bio-inspired photons film with thermoregulatory capability based on dual-scale microstructure proposed by Columbia University, regarded that the triangular hairs can protect its body from overheating through the following methods: 1) high solar reflectivity (61 %) due to Mie resonance and total internal reflection; 2) the special triangle shape of hair can serve as a gradient refractive index layer to enhance the ATW emissivity and increase the radiative heat dissipation to 3 K universe; 3) compared to be covered by hairs, the bare bottom surface can reflect

more MIR radiation emitted by environment.

To reveal the thermophysical mechanism of surviving in high-temperature-equatorial forests, Xie et al. [180] theoretically and experimentally investigated the solar refection and MIR emission property of the scales on the white beetle *Goliathus goliatus*. The schematic illustration of total reflection in the scattering were shown in Fig. 11c. The results indicated that the exquisite shell/hollow cylinder micro-structure of the white scales can significantly increase the solar reflection through thin-film interference, Mie scattering, total internal reflection, and infrared emission enhancement via antireflective layers, which can minimize the solar absorption and maximize the radiative heat dissipation to environment and 3K universe. As shown in Fig. 11d, thermodynamic experimental test indicated that the exquisite shell-/hollow cylinder micro-structure can diminish the body temperature of white beetle up to 7.8 °C, which can provide new inspirations for designing PDRC. Inspired by the longicorn beetles' fluffs due to their superior thermoregulatory capability with dual-scale microstructure, Zhang et al. [181] designed and prepared a bio-inspired photonic film for PDRC, and the preparation and morphology of the bio-RC film were shown in Fig. 11e. The solar reflectivity can reach 95 % and the infrared emissivity can be higher than 96 % of the bio-inspired PDRC film. Outdoor experiment test indicated the bio-inspired PDRC film can achieve a 5.1 °C sub-ambient cooling performance under direct sunlight radiation with a cooling power of 90.8 W/m².

5.3. Photon and phonon-enhanced resonance by cavity or porous

Cavity or porous with a small hole tend to be nearly opaque to electromagnetic radiation and only a small part of this radiation can escape through the hole if the whole is sufficiently small [182,183]. Cavity with a small hole can enhance the vibrations of chemical bond atoms and be approximated as a blackbody, while all incident radiation is absorbed and re-emitted following Planck's law, meaning that it has a spectrum with the function of object temperature alone. Therefore, using micro- and nano-cavities can reach high infrared emissivity easily

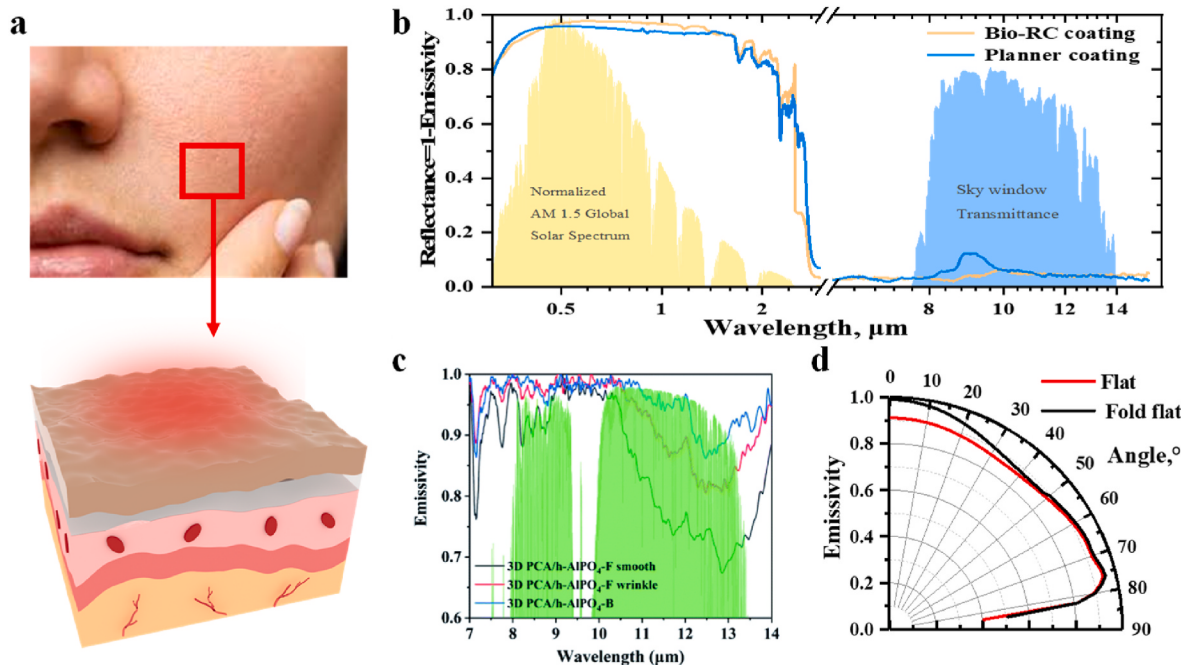


Fig. 10. Bio-skin inspired wrinkle microstructure for efficient spectral radiative property oriented design of both the solar band and ATW band. (a) Photos of human skin (upper panel) and schematic of the skin structure (lower panel) [102]. (b) Tested reflectance (1-emittance) of the bio-PDRC coating and planar coating in normalized ASTM G173 global solar and ATW spectrum [102]. (c) Emissivity in ATW of bio-skin inspired structure PDRC film [177]. (d) Comparison of simulated emissivity in ATW at different incident angles [102]. Figures reproduced with permission from (a, b, and d) Cheng et al., *Nano Energy* 89, 106377 (2021). Copyright 2021 Elsevier; (c) Feng et al., *J. Mater. Chem. A* 9, 25178 (2021). Copyright 2021 the Royal Society of Chemistry.

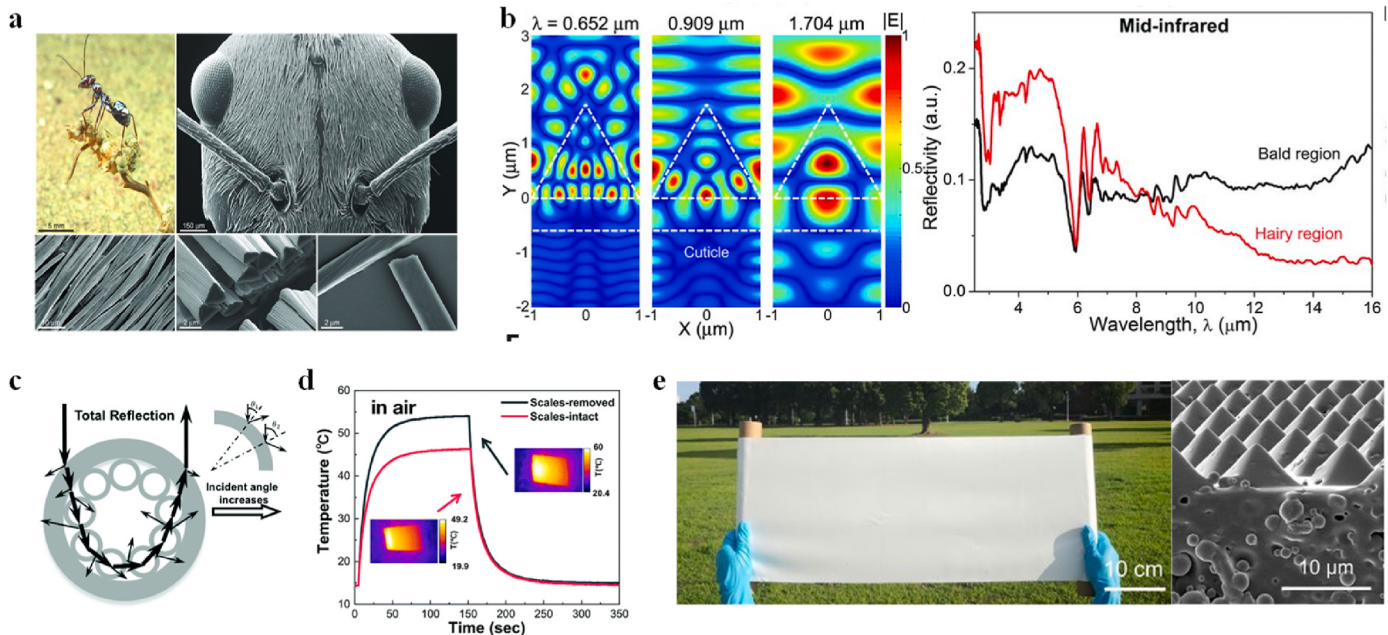


Fig. 11. Bio-inspired photons film with thermoregulatory capability based on dual-scale microstructure. (a) The bright glare of the silver ant and its structural basis [96]. (b) Reflectance of the silver ant's body surface from the visible to the MIR range of the spectrum [96]. (c) Schematic illustration of total reflection in the scattering [180]. (d) Temporal temperature profiles tested for beetle elytra with and without white scales in air [180]. (e) Preparation and morphology of the Bio-RC film [181]. Figures reproduced with permission from (a and b) Shi et al., *Science* 349, 298–301 (2015). Copyright 2015 American Association for the Advancement of Science; (c and d) Xie et al., *Soft Matter* 15, 4294 (2019). Copyright 2019 The Royal Society of Chemistry; (e) Zhang et al., *Proc. National Acad. Sci. U.S.A.* 117, 14657–14666 (2020). Copyright 2020 PNAS.

due to their characteristics of simplified blackbody [184,185].

However, it is hard to achieve high reflection in the solar wavelength band using micro- and nano-cavities. Compared to Mie resonance excited by sphere particles with weak sunlight backward scattering, the size, and shape of the micro- and nano-cavities need to be elaborately designed based on electromagnetic theory, which can exhibit strong sunlight backward scattering with high solar reflectivity. Compared to smooth micro-particles, slab type micro-cavities with eight corners have strong interact with electromagnetic waves and significantly affect the scattering direction. The requirements of strong backward scattering for micro- and nano-cavities to achieve high solar reflection are listed in Table 4. Therefore, micro-cavities with elaborated design can increase the solar reflectivity and ATW emissivity, simultaneously.

Mandal et al. [186] put forward a simple and scalable phase-inversion-based method to prepare hierarchically blended cavities poly PDRC coatings with superior dual-band optical performance and low cost. As shown in Fig. 12a and b, the obtained substrate-independent hemispherical solar reflectance can reach 96 % and the long-wave infrared emittance can reach 97 %, while the optical properties were equal to or higher than the most advanced PDRC

technology. The ultra-high solar reflectivity can eliminate the need for silver reflectors adopted by former designs. The superior dual-band optical properties can realize noteworthy daytime sub-ambient cooling performance under various weathers of Phoenix, New York, and Chatogram. The outdoor experiment tests conducted in Phoenix had achieved a sub-ambient temperature drops of ~ 6 $^{\circ}\text{C}$ and cooling power of ~ 96 W/m^2 under solar intensities of 890 W/m^2 and 750 W/m^2 . Significantly, the phase-inversion-based technique proposed by Mandal can be adapted to a wide variety of polymers for PDRC.

To reveal the relationship between optical properties of PDRC and pore structure, a 2D electromagnetic field calculation model is established and calculated by Chen et al. [187–190] using the finite element method. Fig. 12c ~ e shows the effects of pore radius, porosity, and thickness on the dual-band (solar and ATW) optical property and cooling power were investigated. Chen et al. [61] found that using blended micro-cavities with broad radius distribution can effectively improve the solar reflectance compared to the micro-cavities with single radius. The numerical research conducted by Chen can provide theoretical guidance for designing micro-cavities for PDRC to achieve superior dual-band optical performance [61].

Phase inversion method was adopted by Gao et al. [154,191] to prepare PDRC coating with excellent dual-band optical properties. The high ATW emissivity was achieved by using P(VDF-HFP), while the high solar reflectivity was achieved through the micro-/nano cavities. The reflectance within the visible wavelength range (0.38–0.78 μm) and solar band of a PDRC coating with a thickness of 1000 μm can reach 97 % and 92 %, while its ATW emissivity can reach 96 %. The radiative cooling performance throughout all year was tested, and a maximal sub-ambient radiative cooling temperature drop of 6.9 $^{\circ}\text{C}$ can be reached [75].

A biomimetic radiative property regulation methodology was proposed by Liu et al. [192] for PDRC to realize the goal of scalable preparation and maneuverable form-compatibility to various applications, and the biomimetic photonic multiform composite are shown in Fig. 13. By mimicking the evolutionarily optimized thermoregulatory capability

Table 4
Requirements of strong backward scattering.

Enhancement factors and polarization ratios	Requirements of strong backward scattering
1 Unpolarized enhancement factor	$1 < \xi_1 \leq 2$
2 Co-polarized enhancement	$1 < \xi_{vv} \leq 2$
3 Cross-polarized enhancement factor	$1 < \xi_{hv} \leq 2$
4 Helicity-preserving enhancement factor	$1 < \xi_{hp} \leq 2$
5 Opposite-helicity enhancement	$1 < \xi_{on} \leq 2$
6 Linear polarization ratio	$\mu_L \geq 0$
7 Linear diffuse polarization ratio	$\mu_L^{\text{diff}} \geq 0$
8 Circular polarization ratio	$\mu_C \geq 0$
9 Circular diffuse polarization ratio	$\mu_C^{\text{diff}} \geq 0$

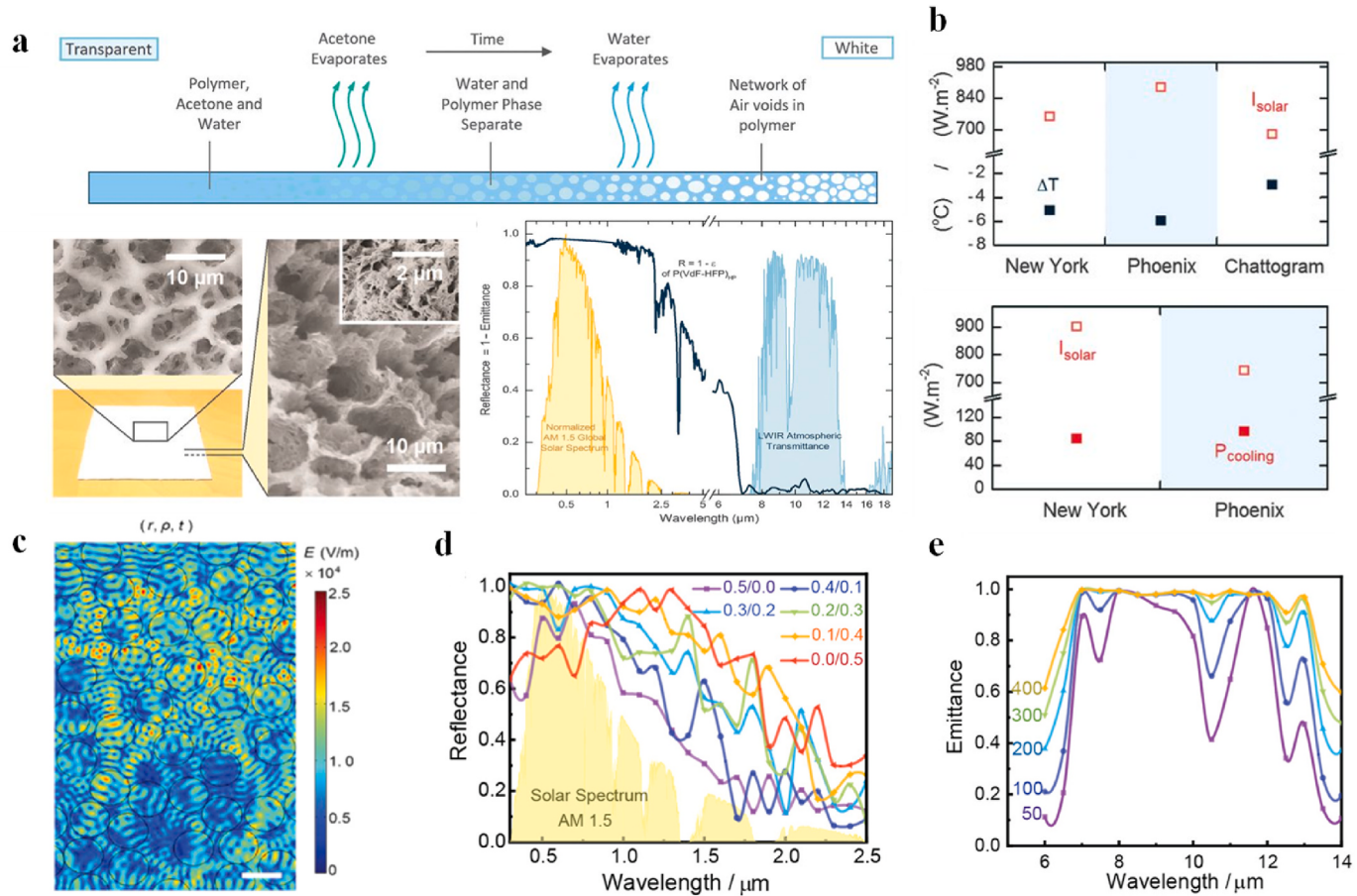


Fig. 12. Designing and fabrication of mesoporous photonic structures for PDRC. (a) The formation and optical properties of hierarchically porous polymer PDRC [186]. (b) The geometry of a porous structure in simulation with the electric field distribution [186]. (c) Schematic diagram of total reflection in the scattering [61]. (d) Effect of the pore size distribution on the reflectance spectra in the solar spectrum [61]. (e) Effect of the structure thickness on the emittance spectra in the infrared region [61]. Figures reproduced with permission from (a and b) Mandal et al., *Science* 362, 315–319 (2018). Copyright 2015 American Association for the Advancement of Science; (c–e) Chen et al., *Nano Lett.* 21, 1412–1418 (2021). Copyright 2021 American Chemical Society.

of golden cicada, a microimprint coupled with phase separation method was formed for preparing PDRC fabric made of porous polymer–ceramic composite profiled in microhumps. Randomly distributed alumina nanoparticles were embedded in the micro-cavities of polymer matrix to obtain efficient Mie scatterings with a superior solar reflectance of 97.6 %, and the ATW emittance can reach 95.5 %. The superior dual-band optical properties can induce a cooling power of 78 W/m^2 and a maximal sub-ambient temperature drop of 6.6°C at noon. A novel viewpoint into design of cavity radius and microspheres' volume percentage for maximized light-scattering air voids and collectively electromagnetic hotspots were put forward by Xiang et al. [193]. Micro-cavities with Mie resonant scattering were designed to reflect sunlight efficiently, while SiO_2 microspheres with phonon-enhanced Fröhlich resonances were designed to dissipate heat to the cold outer space through radiative heat transfer. Fig. 13c shows the experimental results of cooling performance of PPRC cooler under various weather conditions. The average solar reflectance and ATW emittance of the PDRC polymer film can reach 96 % and 95 % with maximum daytime sub-ambient cooling temperature drop of 6.2°C .

6. Application of PDRC technology

6.1. Making and storage ice/iced foods

The International Energy Agency found that 11 % of global electricity consumption was used in refrigeration for food fresh and storage,

which led to 2.5 % of the world's greenhouse gas emissions. Storage ice under direct solar irradiation faced many pressing challenges: 1) due to the lower storage temperature than most applications, it requires ultrahigh radiative cooling power ($70\text{--}110 \text{ W/m}^2$) to prevent ice from melting without any additional refrigerated devices, 2) it should be environment friendly, nontoxic, scalable and low cost.

Fig. 14 shows the passive cooling systems in ancient architecture. About the fourth century BC, Persian utilized the principle of passive radiative cooling to construct yakhchâls (an ancient type of ice house) in the desert to make and store ice. In the desert, especially the places located at high altitudes, the clear sky causes hot during the day while it can be used as a superior heat sink at night. On a clear night, substances facing the sky can dissipate heat to the cold space through passive radiative cooling. Hence, even if the ambient temperature surpasses the freezing point of water, the temperature of the water in the yakhchâls can be lowered to below 0°C , causing it to freeze [194,195]. This principle can also explain the phenomenon of frost on the car windshield in the morning of late autumn.

Jinlei et al. [197] proposed a hierarchically designed PDRC film for ice storage under direct solar irradiation. Cellulose acetate was used to build the hierarchically PDRC film, which can be extracted from natural cellulose that existed extensively within plant cytoderm and eco-friendly. The inherent vibrations of the molecular bonding endow the hierarchically PDRC film with broadband and high ATW emissivity with the value of 92 %, while the weighted solar reflectivity can reach 97.4 %. A maximum cooling power of 110 W/m^2 and a peak

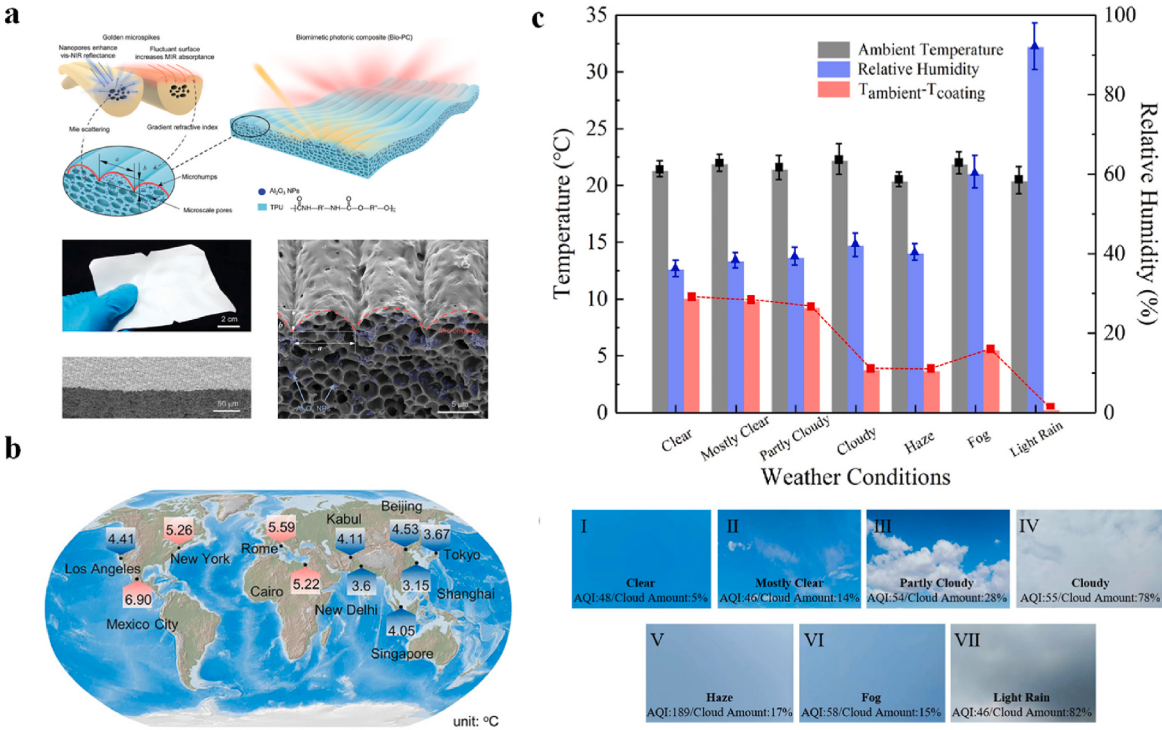


Fig. 13. Outdoor application of radiative cooling materials in different climates. (a) Biomimetic photonic multiform composite obtained by Liu et al. [192]. (b) Predicted maximum ΔT of radiative cooling cooler for different cities [192]. (c) The experimental results of cooling performance of PPRC cooler under various weather conditions [75]. Figures reproduced with permission from (a and b) Liu et al., *Adv. Opt. Mater.* 362, 315–319 (2018). Copyright 2018 Wiley; (c) Gao et al., *Sol. Energy* 228, 474–485 (2021). Copyright 2021 Elsevier.

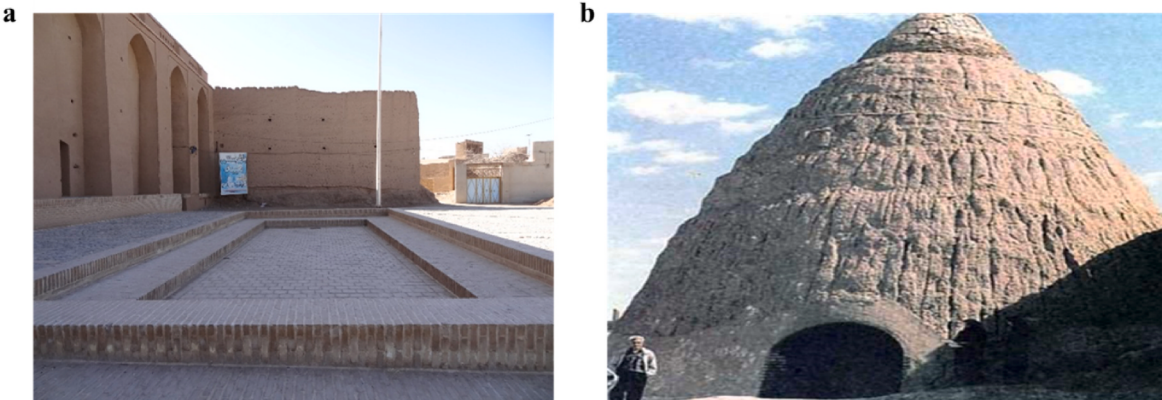


Fig. 14. Passive cooling systems in ancient architecture. (a) An ancient type of ice house (Yakhchals) constructed by Persian scientists [194]. (b) Domed roof fridge in Razavi Khorasan Province, Iran [196].

sub-ambient cooling temperature of $\sim 12^{\circ}\text{C}$ were achieved by the hierarchically designed PDRC film under direct solar heating. The experimental test showed that the preservation time of the iced food wrapped by hierarchically designed PDRC film can reach 5.5 h, which was much longer than those wrapped by the white paper, Al film, and PET-Al-PE film (3.7, 3.8, and 2.6 h).

Theoretically, the sub-ambient temperature drop can reach 60 K by using radiative cooling technique to dissipate heat to outer space. The critical influences of achieving such ultra-high sub-ambient temperature drop is to employ greatly selective thermal emitter matched to the ATW, and minimize parasitic thermal load [198]. To achieve deep sub-freezing temperatures through a 24-h day-night cycle, Shanhui et al. [199] designed and manufactured an apparatus composed of a

selective thermal emitter encompassed by a vacuum chamber to shield it from direct solar heating. The apparatus needed to guarantee that the selective emitter was thermally decoupled from the ambient air and the sun, while coupled to the cold outer space via the ATW. As shown in Fig. 15, under a 24 h day-night cycle, the apparatus designed and manufactured by Shanhui et al. [199] reached an amazing maximum sub-ambient cooling temperature of 42°C and an average sub-ambient cooling temperature of 33°C , which was very promising for making and storage ice.

6.2. Energy conservation in buildings

Amidst rapid growth of population and economy, the challenge of

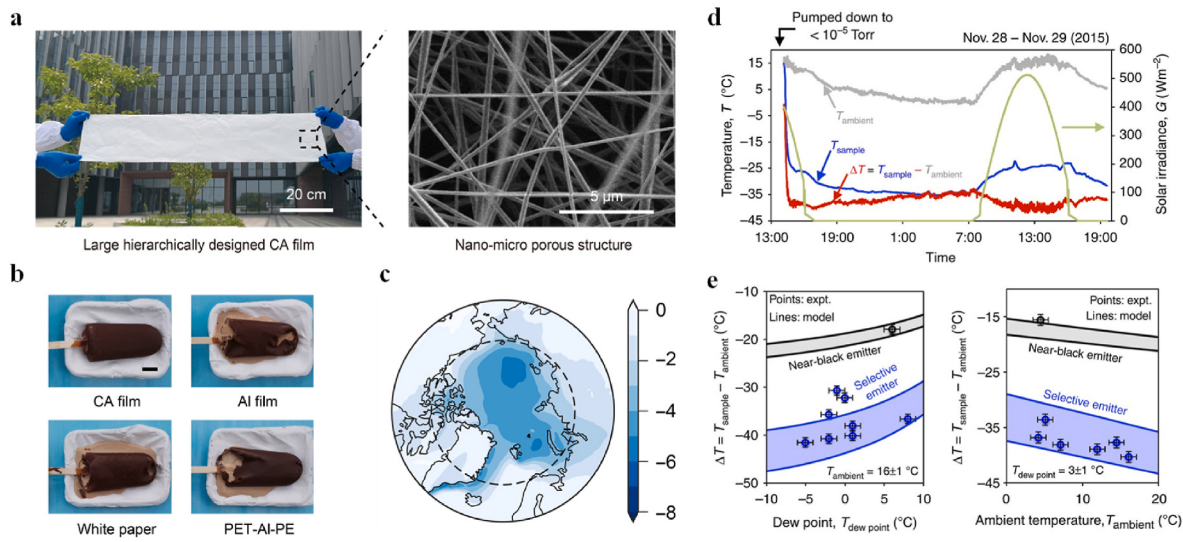


Fig. 15. The outdoor application of radiative cooling materials in different climates. (a) Hierarchically designed cellulose acetate film for outdoor ice/ice-food preservation [197]. (b) Sunlight-exposed photos of the ice creams after 80 min [197]. (c) Maps of the differences in surface temperature of cellulose acetate film with and without hierarchically designed, respectively [197]. (d) Large sub-ambient temperature through radiative cooling in a 24 h day-night cycle [199]. (e) Selective emitter with low dew point and high ambient temperature can achieve large temperature reduction through radiative cooling [199]. Figures reproduced with permission from (a–c) Li et al., *Sci. Adv.* 362, 315–319 (2018). Copyright 2018 American Association for the Advancement of Science; (d and e) Chen et al., *Nat. Commun.* 7, 13729 (2016). Copyright 2016 Springer Nature Limited.

addressing the escalating demands for building heating and cooling energy has emerged as a formidable global predicament [200–202]. Taking the USA as an example, nearly 40 % of the total energy consumption was in buildings to pursue a comfortable indoor temperature. In particular, energy consumption for cooling accounted for up to 30 %–50 % of total building energy consumption for the residential housing energy portion, especially in summer and hot areas [203–205]. The energy burden of building cooling has become a global challenge due to the deteriorative phenomena of global warming and the unbalance influence on end-use energy consumption and peak load [206–209].

To evaluate the global energy saving potential of using the radiative cooling technique, Joseph et al. [210] proposed a high-fidelity radiative cooling evaluation model which considered atmospheric factors including precipitation, atmospheric transparency, and wind-induced dynamic convective heat transfer coefficient. Joseph et al. [210] enforced the radiative cooling evaluation model for single-story residential buildings to research the influence of radiative cooling in all the ASHRAE climate zones in the USA. The numerical analyses indicated that over 22 % and 46 % power savings in warm climates for high efficiency building and typical building can be achieved by using the PDRC technique. Amir et al. [211] developed a whole-building energy analysis model to evaluate the potential of using the “radiative cooling technique” on conventional rooftops of archetypical residential and commercial buildings. The numerical analyses indicated that the rooftop surface temperature can reach sub-ambient temperature cooling almost all the year and yielding a negative average daily sensible heat flux of 30~40 W/m². By using the radiative cooling technique on the rooftops, the overall energy expenditure in commercial buildings and residential buildings can be reduced up to 19 % and 28 %, respectively [212–214].

Dongliang et al. [215] proposed a novel concept of a roof-integrated radiative air-cooling system, which combined the techniques of radiative cooling and attic ventilation to decrease the attic temperature. A radiative air cooler model with the surface area of 1.08 m² was manufactured and tested in outdoor environment. Day-night continuous sub-ambient cooling of air had been obtained under three different flow rates on summer days, which had never been reported before. The maximum sub-ambient temperature drop can reach 8 °C at night and

5 °C at noon, respectively. The annual cooling energy savings by using the roof-integrated radiative air-cooling system can reach 3.7 kWh/m²~11.8 kWh/m² (26.5 %–76.1 %) [215].

Cheng et al. [102] put forward the methodology of using biomimetic wrinkle structure combined with optimized particles to regulate the dual-band optical properties of PDRC. The prepared bio-PDRC coating with a thickness of ~100 μm can reach 95 % solar reflectivity and 96 % ATW emissivity. A comprehensive year-long outdoor architectural application verified the energy conservation performance of the bio-PDRC coating Fig. 16 shows the comparison of experimental results of buildings with/without Bio-RC coating. The experimental test was conducted at noon on August 17th, 2020 and showed that the maximum temperature drop can reach 23.6 °C by covering bio-PDRC coating. Besides, Cheng et al. also conducted a whole year radiative cooling performance with the monitor of roof surface and indoor air temperatures. Figs. 16c and e presented that the bio-PDRC coating also exhibited superior energy conservation performance for buildings: in summer, the average indoor air temperature drop can reach 6.2 °C, while the average indoor air temperature drop in winter was only 0.3 °C and almost unchanged. By spraying bio-PDRC coating on roof of buildings, the net energy saving conservation of a whole year can reach 48 kWh/m², and the net energy conservation in dry and hot areas can be larger.

6.3. Fresh water preparation

Atmospheric water vapor is regarded as an alternative resource of freshwater in drought regions such as deserts, islands, and remote areas due to its vast total amount and universal accessibility [216–218]. Water vapor condenses when its temperature decreases below the dew point. If the dew point is lower than the air temperature in the environment, only radiative transfer can further chill-down the condenser since conductive and convective heat transfer drives the condenser temperature toward the environmental temperature [219,220]. Atmospheric water vapor condensation is a universal phenomenon existing in nature [221–223]. For example, when the atmospheric humidity is high enough at night, insect's elytra can spontaneously cool itself to below dew point by radiating thermal energy via ATW to outer cold space (known as night-time radiative cooling). Nevertheless, this cooling technique

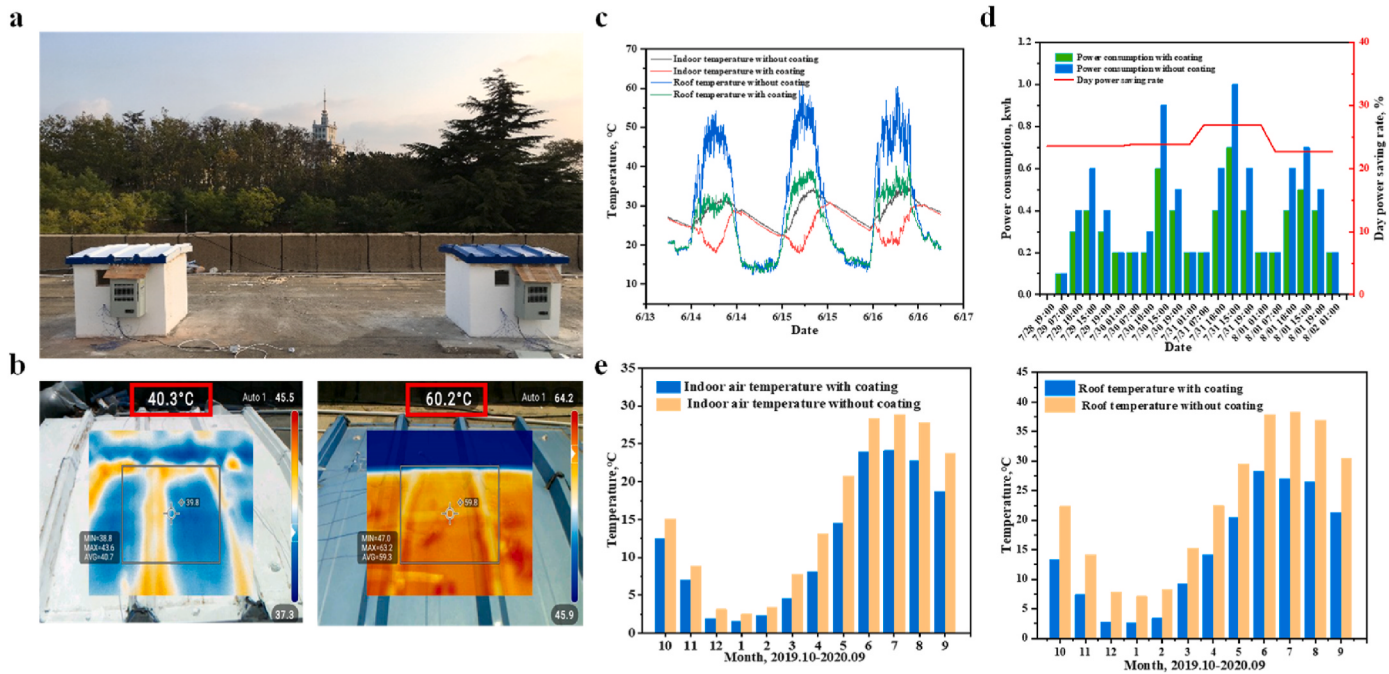


Fig. 16. Comparison of experimental results of buildings with/without Bio-RC coating [102]. (a) Photograph of the two tested buildings with air-conditioners. (b) Infrared thermal images of the building roof painted with and without the Bio-RC coating. (c) Building continuous temperature test curve. (d) The air-conditioning electricity consumption graph for each period. (e) Comparative experimental result of the monthly average roof temperature and indoor air temperature. Figures reproduced with permission from (a–e) Cheng et al., *Nano Energy* 89, 106377 (2021). Copyright 2021 Elsevier.

cannot be compatible with solar water-purification technique, since the power of solar heating was much larger than that of night-time radiative cooling.

Due to the large consumption of fossil fuel or electricity in conventional condenser, passive vapor condensation using PDRC technology becomes especially promising. Iwan et al. [224] presented an atmospheric water collecting technique with superior-performance, full passive and unremitting 24-h water collection that was driven by radiative cooling under atmospheric conditions. As shown in Fig. 17a, under direct sunlight at realistic relative humidity levels, an elaborately manufactured radiative cooling shield was used to harvest the daytime atmospheric water with collected dew mass fluxes up to $50 \text{ g}/(\text{m}^2 \cdot \text{h})$, which approached the limit capability of such system.

Inspired by the special hydrophilic and hydrophobic patterns on the dorsal surface of the Namib Desert Beetle for harvesting water from air, vein-like patterned surface was adopted by Qiuyue et al. [225] to improve the water collection efficiency from atmospheric air in desert. As shown in Fig. 17b, $\text{MgHPO}_4 \cdot 0.78\text{H}_2\text{O}$ functional particles were prepared and added in the radiative cooling layer to act as a cooling function on the backside of the water-collection layer, which can provide additional capabilities of decreasing the re-evaporation rate and improve water harvesting efficiency. Benefitted from PDRC technique, the efficiency of water collection can be improved by $198.51 \text{ mg}/(\text{cm}^2 \cdot \text{h})$, and the efficiency of water collection of a retrofitted condenser with bilateral-sided functional structure was 67.33% higher than that harvested by a smooth aluminum condenser. Guoliang et al. [226] had prepared a wettability and spectral selectivity engineered coating for efficient water harvesting from atmospheric vapor, which coupled the PDRC and dropwise harvesting strategies. The multifunctional coatings were prepared by mixing hydrophobic SiO_2 and hydrophilic TiO_2 nanoparticles with a fluorine resin adhesive using a scalable and low cost preparation procedure. The multifunctional coatings can reflect almost 90 % of the incoming solar irradiation and can emit over 95 % of long wavelength electromagnetic radiation to the outer cold space, and it can spontaneously cool itself to below the dew point under high humid condition under direct sunlight. As shown in Fig. 17c, atmospheric water

vapor can be condensed on the multifunctional coating and discrete water droplets were harvested.

To research the impact of radiative cooling on the production rate of solar desalination, Amarloo et al. [227] proposed, manufactured and measured an innovative solar distiller with two exterior condensers. Fig. 17d shows the structure of the solar distiller: one condenser was filled with phase change materials and cooled by radiative cooling at night, while the other condenser was cooled by natural convective heat transfer with environment. In the daytime, solar collectors were used to collect the incoming solar irradiation and heat the seawater. Inside the evaporation cistern, the evaporated vapor was diverted to the exterior condensers and was chilled in the other condenser by transferring heat with the stored sky coldness in phase change materials, and in the other condenser by transferring heat with environment through convective heat transfer.

6.4. Personal thermal management

As warm-blooded animals, human evolved endotherm organisms to biologically regulate its body at a metabolically favorable temperature [228–231]. Maintaining the core body temperature at a comfortable temperature was the primary need for living conditions, which was commonly obtained by air conditioning of a whole room or building with a great deal of energy consumption, accounting for fifteen percent of the whole electricity consumption of the world. Compared to the whole room or building, human body has extremely small heat capacity. The purpose of personal thermal management (PTM) is strategy to serve cooling or heating only to the core body and by which to extend room temperature set point range for huge energy conservation [232–234].

Departing from the temperature regulation by an air conditioner, clothes made by various fabrics and textiles became the unique method to regulate the temperature of core body. Nevertheless, conventional fabrics and textiles had limited function of thermal insulation, which cannot achieve sub-ambient temperature cooling through PDRC technology. Several advanced studies had been conducted to improve the thermal radiation from the human body to the environment through

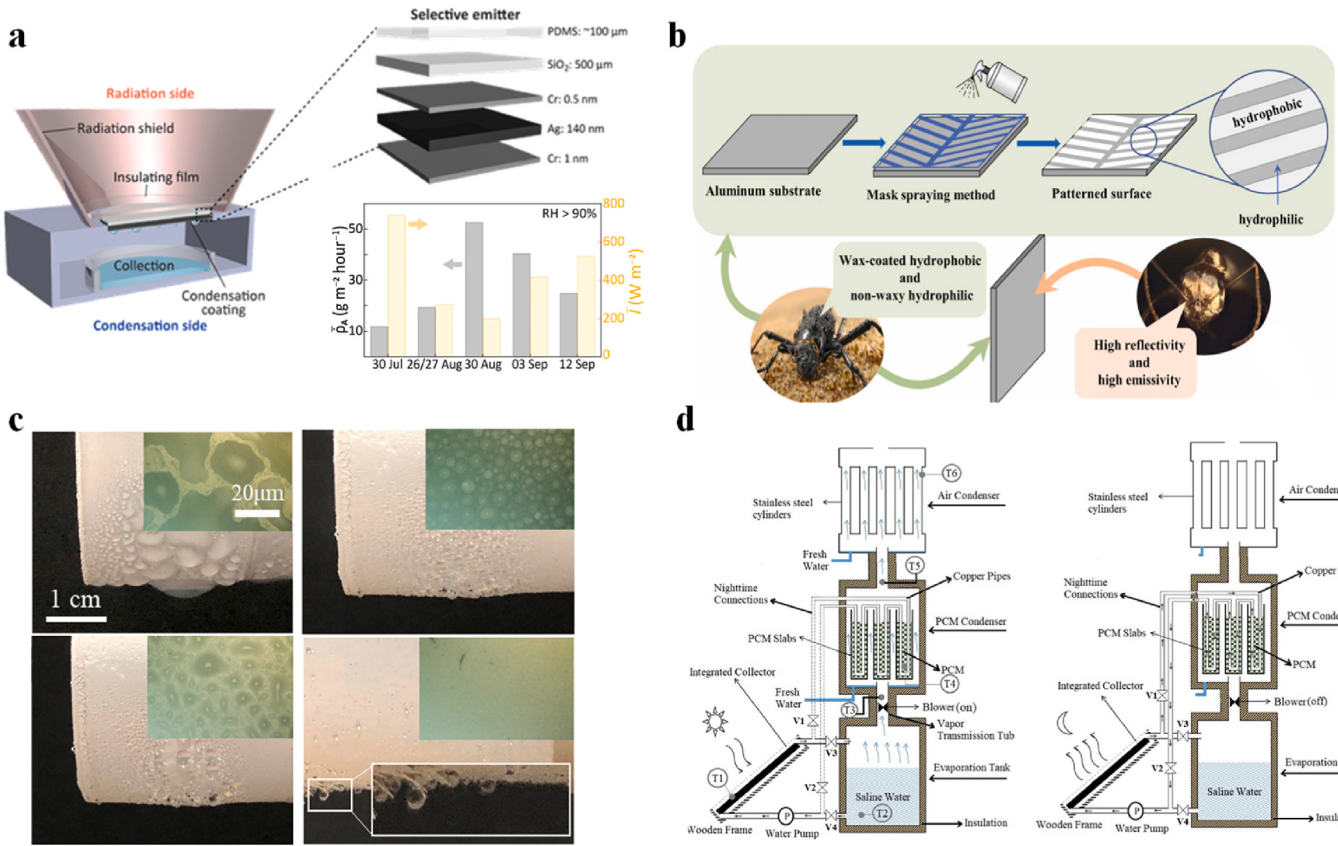


Fig. 17. Fresh water preparation by radiative cooling. (a) Multi-layer selective transmitter for continuous 24-h water collection [224]. (b) Patterned hydrophilic-hydrophobic surface for efficient water harvesting [225]. (c) Water collection on different radiant cooling surface [226]. (d) The solar still condensation is enhanced by using PDRC system and phase change material in daytime and nighttime [227]. Figures reproduced with permission from (a) Haechler et al., *Sci. Adv.* 362, 315–319 (2021). Copyright 2021 American Association for the Advancement of Science; (b) Wang et al., *Colloid Surf. A-Physicochem. Eng. Asp.* 658, 130584 (2023). Copyright 2023 Elsevier; (c) Chen et al., *Mater. Des.* 206, 109829 (2021). Copyright 2021 Elsevier; (d) Amarloo et al., *Desalination* 467, 43–50 (2019). Copyright 2019 Elsevier.

high infrared electromagnetic wave transmission fabrics. However, using the environment as a heat sink thermodynamically restricted the probability of achieving sub-ambient temperature cooling. When the human body was outdoors, the cold outer space can be a much better heat sink compared to the ambient environment (3 K < 300 K). Herein, improved fabrics with super-high ATW emissivity had the probability of achieving sub-ambient temperature cooling for PTM [235,236].

Zeng et al. [120] developed a PDRC textile weaved by composite microfibers with multi-layers, of which a 500 μm TiO₂-PLA woven fabric was overlaid with a PTFE layer, the design principles and practical application effects of PDRC textile were shown in Fig. 18a–c compared with cotton-covered textile, the PDRC textile can decrease temperature of simulated skin to 4.8 °C. However, conventional PDRC hydrophobic materials with large thickness had poor moisture management, which can induce core body uncomfortable and insufficient cooling effects during sweating for personal thermal management. Nanoporous polyethylene (PE) film had the properties of transparent in visible wavelength, breathability, and low moisture absorption, which were not suitable for making clothes. Po-Chun et al. [237] successfully modified the optical properties of PE by using interwoven nanoporous structure, which had high infrared electromagnetic wave transmission and didn't permit visible electromagnetic wave transmission. The apertures of nanoporous were approached to the wavelength of visible electromagnetic wave, which can scatter the visible light backward effectively and made it opaque to human eyes. While the aperture of nanoporous were one order of magnitude smaller than the wavelength of infrared radiation emitted by a human body. Therefore, the nanoporous structure can not affect the intrinsic optical properties of PE film with high infrared

electromagnetic wave transmission. Fig. 18d confirms the excellent breathability and tensile strength of nanoporous materials Cai et al. [238] prepared a novel PDRC metafabric using ZnO micro-particle embedded PE which decreased the temperature of imitated core body to 5–13 °C compared with conventional fabric. To overcome the drawback of low moisture penetration, Xiaoshuang et al. [239] had proposed a kind of moisture-wicking PDRC hierarchical metafabric based on nanofiber membrane, which combined PDRC technique and wick-evaporation cooling to realize efficient thermal and vapor management simultaneously. The fabricated moisture-wicking PDRC hierarchical metafabric had two layers: CA/Al₂O₃/HPX layer and PA₆/SiO₂/HPX layer, which can induce a moisture gradient and push the vapor to be evaporated quickly. Cooling performance tests indicated that wearing an imitated human body with the PDRC hierarchical metafabric had good capability of vapor penetration and can inhibit overheating by 16.6 °C compared with conventional fabrics.

To keep the core body persistent comfortable under cyclical changed weather, the method of dual-mode fabric for radiative cooling and heating was proposed by Po-Chun et al. [240] to withstand the fluctuating environmental temperature variation, the schematic and experiences of the dual-mode radiative cooling material were shown in Fig. 19, which was made by a multilayer radiator embedded inside an infrared-transparent nanoporous PE layer. As a result of the asymmetrical characteristics of both emissivity and nanoporous PE thickness, disparate electromagnetic transfer responses were observed. The laws of thermodynamics ensured the occurrence of thermal radiation that net-emits from a hotter substance to the cooler environment, while the radiative dual-mode fabric had an extensive range of applications

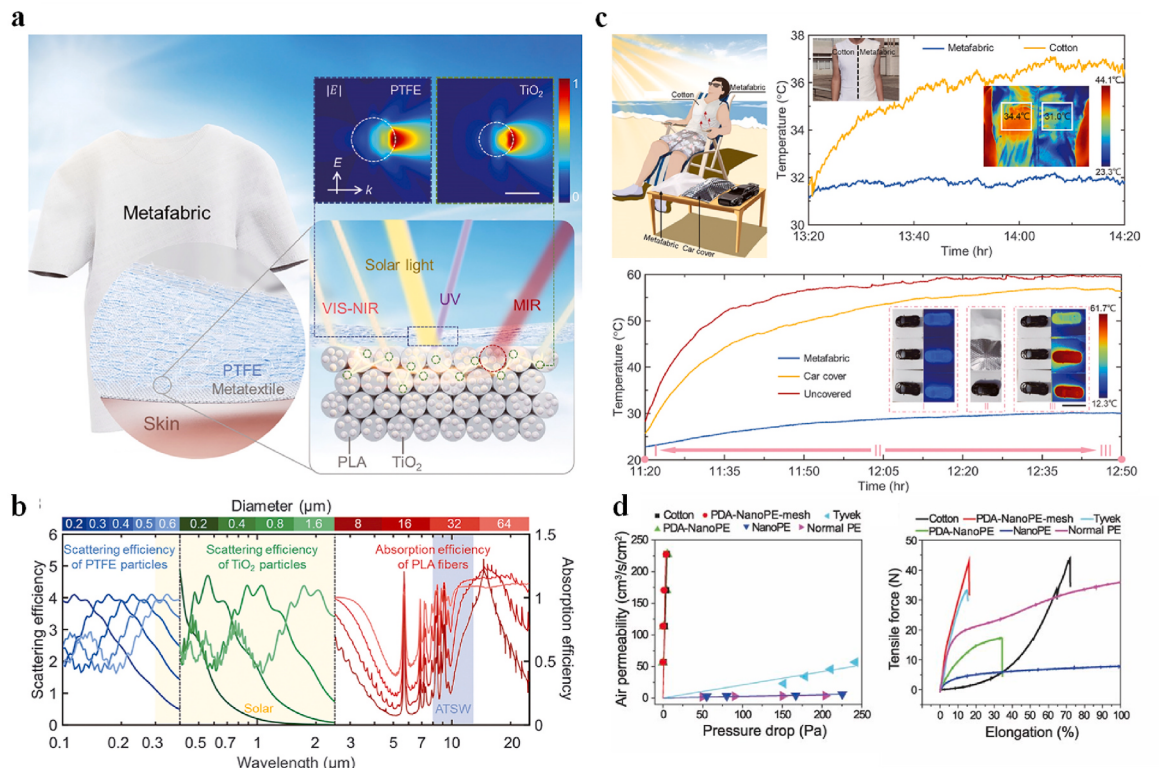


Fig. 18. PDRC for personal thermal management. (a) Multilayer metafabric knitted to integrate PDRC technology for personal thermal management application [120]. (b) Hierarchical-morphology design mechanism enhances spectroscopic response [120]. (c) Practical characterization of metafabric application in human body and model cars [120]. (d) Air permeability test (left panel) and tensile strength test (right panel) of nanoporous PE textile prepared by Hsu et al. [237]. Figures reproduced with permission from (a–c) Zeng et al., *Science* 373, 692–696 (2021). Copyright 2021 American Association for the Advancement of Science; (d) Hsu et al., *Science* 353, 1019–1023 (2016). Copyright 2016 American Association for the Advancement of Science.

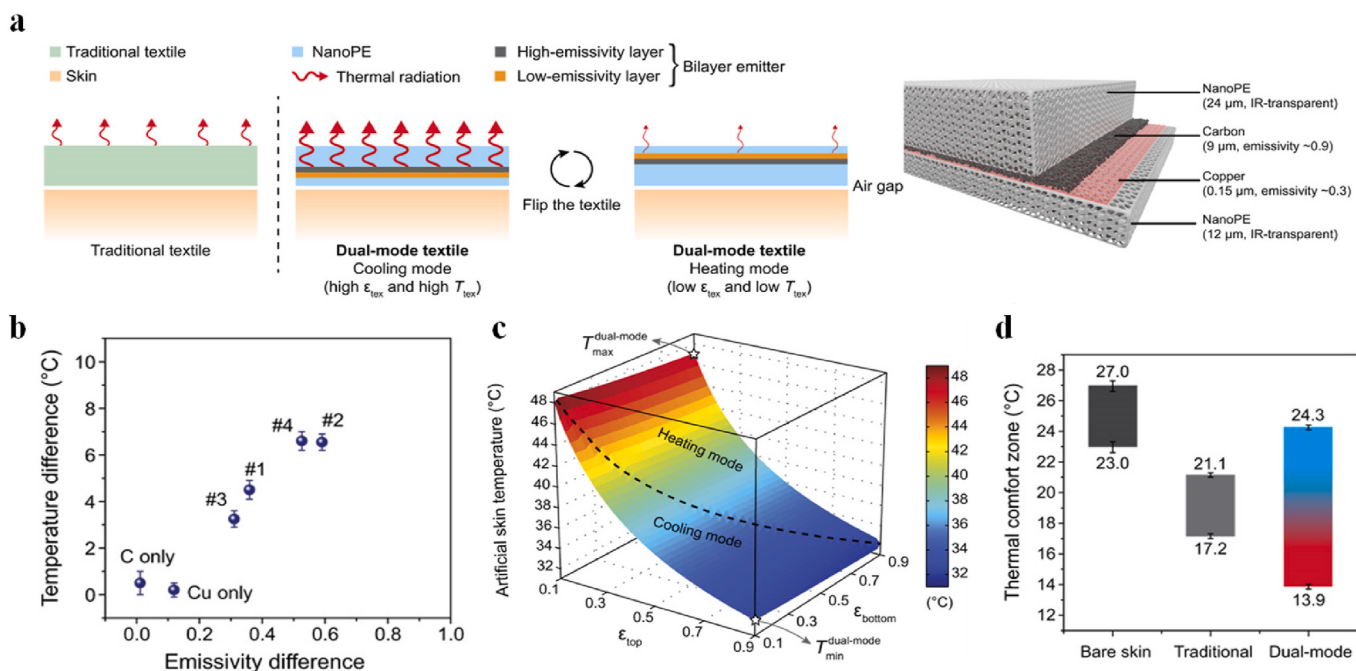


Fig. 19. Dual-mode radiative cooling material for heating and cooling of human body [240]. (a) Schematic (left panel) and layered structure (right panel) of dual-mode radiative cooling material obtained by Hsu et al. [240]. (b) Mode switching of two layers results in a positive relationship between temperature difference and emissivity difference. (c) Functional between temperature of human skin and emissivity of top and bottom layer. (d) Comparison of thermal comfort zones of different surfaces. Figures reproduced with permission from (a–e) Hsu et al., *Sci. Adv.* 3, e1700895 (2017). Copyright 2017 American Association for the Advancement of Science.

without the need of additional energy input or clothes, such as: social, utility, and protection [240].

6.5. Thermoelectric generation

Electricity, a highly adaptable form of intangible energy, has revolutionized various facets of human life and production patterns [241, 242]. Using capturing sunlight, daytime electricity power generation using photovoltaic (PV) cells has achieved significant improvement over the past half century [243–245]. Thermoelectric generators (TEG) can harvest power from converting thermal energy using a temperature gradient into electricity energy by the seebeck effect [246, 247]. TEG has the advantages of non-mechanical vibration, superior durability, excellent working process reliability, and 24-h electricity -generation [248, 249]. An effective approach to increase the electricity generation efficiency was to enlarge the temperature differences between the heat and cold TEG ends [250, 251]. Conventional techniques to reduce the temperature of TEG cold ends were confined to cooling by means of fluid (i.e. air, water, and heat-transfer oil) flow. However, fluid flow cooling methods had the drawbacks of large size, low heat transfer rate, and consumption of fuel or electricity, which resulted in electricity loss and TEG conversion efficiency decrease. Therefore, seeking a passive cooling technology without consuming any energy for TEG cold end was a promising strategy. The ultra-cold outer space can be an ideal heat sink, and the combination of radiative cooling technology with TEG can achieve efficient passive electricity generation, especially for those applications with power demands at night [252, 253].

Aaswath et al. [254] were the pioneer of harvesting the cooling energy from cold outer space through radiative cooling technology to produce electricity power with a ready-made TEG. The cold end of the TEG was painted with commercial radiative cooling coating ($\varepsilon_{\text{Atm}} = 0.95$) and faced to sky, which can radiate long wavelength infrared energy to the cold outer space effectively. The temperature differences between the heat end and cold end could reach 6.5 °C by harvesting the

cold energy from outer space, and the maximum generated electricity power was 25 mW/m². Therefore, Aaswath had theoretically and experimentally demonstrated the possibility of enabling electricity generation using TEG at night.

Conventional TEG system coupled with radiative cooling had the shortcomings of energy consumption in hot end, intermittent electricity output, and low power generation. To get rid of the drawbacks, Cunhai et al. [255] proposed the idea of coupling the greenhouse and PDRC techniques to realize a passive TEG system with continuous 24-h day electricity generation. The cold end of TEG was placed to face the sky to use the radiative cooling effect and in turn decreasing the temperature. The hot end of the TEG was placed to face the ground and set into a greenhouse fabricated by optical selective polyolefin films, and the temperatures inside greenhouses can be higher than ambient temperatures due to the outstanding greenhouse effect. Therefore, the combination of PDRC technique and greenhouse effect can increase the temperature difference between hot end and cold end of the TEG, which can improve the electricity generation efficiency. As shown in Fig. 20, the novel passive TEG device put forward by Cunhai et al. [255] had been experimentally built and validated the electricity generation performance through all-day continuous test. The experimental test indicated that the novel passive TEG device can generate electricity power of 90.74 mW/m² in a 24-h test cycle.

Furthermore, Cunhai et al. [256] proposed to use the incoming sunlight to heat the greenhouse, and in turn further increase the temperature difference between the hot end and cold end of passive TEG device, especially in the daytime. As shown in Fig. 21, The effects of solar radiation intensity, optical properties of PDRC, and weather conditions on electricity generation efficiency were theoretical and experimental investigated in detail. In Beijing, the average 24-h continuous electricity generation in a summer day was 1050 mW/m², nearly the twice as much as the 570 mW/m² in a spring day and 610 mW/m² in an autumn day. Even in a winter day, the novel passive TEG device can generate a 24-h average electricity production of 270 mW/m². The

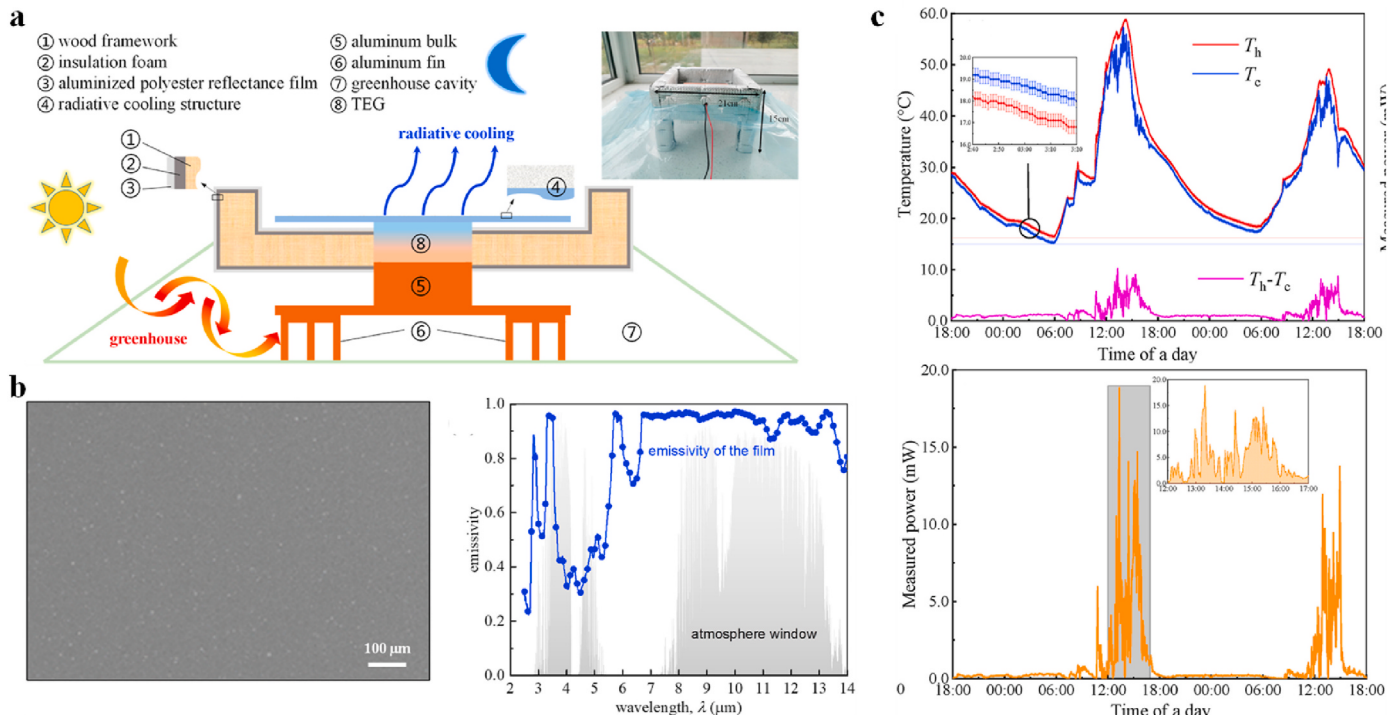


Fig. 20. Passive TEG system combining radiative cooling technology and greenhouse effects obtained by Cunhai et al. [255]. (a) Schematic and experiment setup of thermoelectric system. (b) Electron micrograph (left panel) and emissivity (lower panel) of the radiative cooling film. (c) Temperature (upper panel) and output power (left panel) of the passive TEG system. Figures reproduced with permission from (a-c) Wang et al., *Energy* 263, 125735 (2023). Copyright 2022 Elsevier.

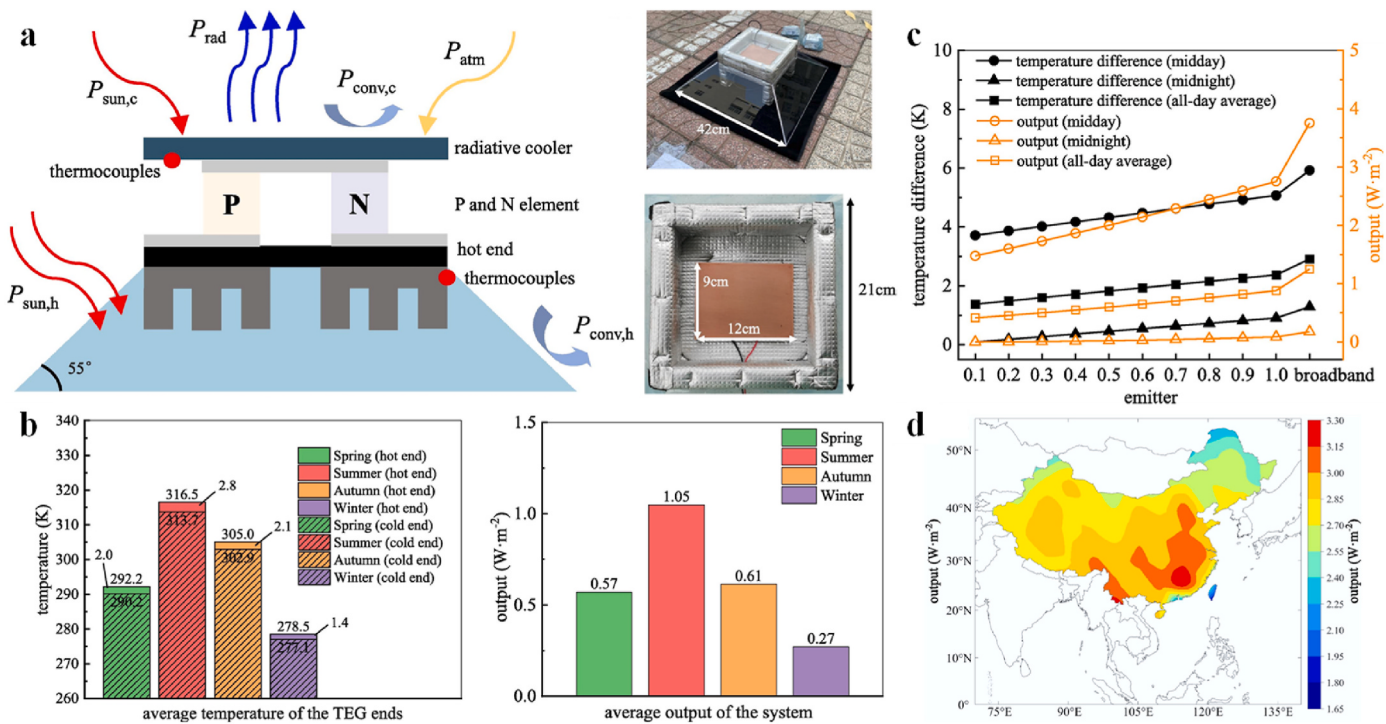


Fig. 21. Performance evaluation of passive thermoelectric system [256]. (a) Schematic of passive TEG system. (b) Full-day performance for different seasons: temperature of TEG (left panel) and output (right panel). (c) The temperature difference and output of TEG system. (d) The max output of passive TEG system in China. Figures reproduced with permission from (a-d) Wang et al., *Appl. Energy* 331, 120425 (2023). Copyright 2022 Elsevier.

seasonal and positional performance of the novel passive TEG device in China was assessed. From the electricity generation map in China, a maximum electricity generation of 3290 mW/m^2 was obtained by the novel passive TEG device when the device was placed at Shaoguan, Guangdong province. Overall, the novel passive TEG devices proposed by Cunhai et al. [254,256] can integrate the strategies of PDRC, greenhouse effect, and solar heating, and can be a benefit for off-grid scenarios which demanded continuous low-electricity supply without any additional fossil fuel energy input.

7. Conclusion and future development

This article presented a review on the fundamental physics mechanism of PDRC technology. Detailed discussions are conducted on methods such as infrared absorption functional group selection, optical band gap selection for solar reflection, photon and phonon enhanced resonance by micro-structure. These discussions offer comprehensive guiding strategies to enhance radiative cooling power. This article also reviewed the progress of PDRC related applications. Using the 3 K cold outer space as a heat sink, PDRC technology can reach sub-ambient temperatures even at peak hours, making it exceptionally applicable in areas like ice/food production and storage, building energy conservation, freshwater generation, personal thermal management, thermoelectric power generation, and spacecraft thermal control.

Although PDRC technology, as an environmentally friendly and promising passive cooling technology, can achieve sum-ambient temperature cooling without consuming any additional energy, its large-scale application is still limited. The drawbacks of low radiative cooling power, single function of cooling, and high whiteness requirement restricted the application of PDRC technology. These challenges also present inspiration and opportunities for PDRC's future development, the following techniques can be developed for PDRC in the future:

- Using a concentrator to amplify the radiative cooling power. Since the current maximum emissivity of PDRC technology in the ATW

band has reached 98 % and approaches the ideal value, it is very hard to further increase the ATW emissivity. A concentrator with highly reflective inner surfaces can be installed to utilize more downward radiations from the atmosphere along the directions away from the zenith direction.

- Color extensibility with ultra-high solar reflectance. To pursue ultra-high solar reflectance, conventional PDRC cooler adopt white color to minimize solar radiation absorption. However, the color appearance requirements in practical scenarios for PDRC cooler are diversified. Herein, it is necessary to extend color diversity with ultra-high solar reflectance for PDRC techniques to fulfill the application demands.
- Smart temperature adaptive PDRC technology. Conventional PDRC technology can achieve sub-ambient cooling in hot summer, but it can also cool the terrestrial substances in cold winter which needs heating. Therefore, it needs to develop temperature adaptive PDRC technology, which can realize smart sunlight reflection and ATW emission regulation with temperature variation.

Overall, PDRC technology is well-established that it is a promising technique to achieve passive cooling for the application of making/storage ice/iced foods, energy conservation in buildings, fresh water preparation, personal thermal management, thermoelectric generation, and thermal management in spacecraft. Amid growing global concerns over energy crisis and environmental pollution, PDRC technology holds the promise of playing a more significant role addressing energy scarcity, mitigating global warming, and offering valuable guidance for policymakers.

Declaration of competing interest

The authors declare that they have no known competing financial interests or personal relationships that could have appeared to influence the work reported in this paper.

Data availability

No data was used for the research described in the article.

Acknowledgements

This work was supported by the National Natural Science Foundation of China (grant 52076064 and 52211530089), Taishan Scholars of Shandong Province grant (tsqn201812105), and The Royal Society (IEC/NSFC/211210). A very special acknowledgment is made to the editors and peer reviewers who provided important comments that improved this paper.

References

- [1] Nastasi B, Markovska N, Puksec T, Duić N, Foley A. Renewable and sustainable energy challenges to face for the achievement of Sustainable Development Goals. *Renew Sustain Energy Rev* 2022;157:112071.
- [2] Jia T, Huang J, Li R, He P, Dai Y. Status and prospect of solar heat for industrial processes in China. *Renew Sustain Energy Rev* 2018;90:475–89.
- [3] Hu M, Zhao B, Suhendri Ao X, Cao J, Wang Q, et al. Applications of radiative sky cooling in solar energy systems: progress, challenges, and prospects. *Renew Sustain Energy Rev* 2022;160:112304.
- [4] Loni R, Mahian O, Markides CN, Bellos E, Le Roux WG, Kasaeian A, et al. A review of solar-driven organic Rankine cycles: recent challenges and future outlook. *Renew Sustain Energy Rev* 2021;160:111410.
- [5] Farooq AS, Zhang P, Gao Y, Gulfam R. Emerging radiative materials and prospective applications of radiative sky cooling - a review. *Renew Sustain Energy Rev* 2021;144:110910.
- [6] Wang FQ, Dong Y, Li Y, Xu J, Zhang GL. Numerical study on the thermal performance of packed-bed latent heat thermal energy storage system with biomimetic alveoli structure capsule. *Sci China Technol Sci* 2021;64:1544–54.
- [7] Shi X, Wang F, Cheng Z, Liang H, Dong Y, Chen X. Numerical analysis of the biomimetic leaf-type hierarchical porous structure to improve the energy storage efficiency of solar driven steam methane reforming. *Int J Hydrogen Energy* 2021;46:17653–65.
- [8] Tian Y, Liu X, Luo Q, Yao H, Wang J, Dang C, et al. Sea urchin skeleton-inspired triply periodic foams for fast latent heat storage. *Int J Heat Mass Tran* 2023;206:123944.
- [9] Zhang Y, Qiu Y, Li Q, Henry A. Optical-thermal-mechanical characteristics of an ultra-high-temperature graphite receiver designed for concentrating solar power. *Appl Energy* 2022;307:118228.
- [10] Liang H, Wang F, Yang L, Cheng Z, Shuai Y, Tan H. Progress in full spectrum solar energy utilization by spectral beam splitting hybrid PV/T system. *Renew Sustain Energy Rev* 2021;141:110785.
- [11] Liu B, Ma L, Feng H, Zhang Y, Duan J, Wang Y, et al. Photovoltaic-powered electrochemical CO₂ reduction: benchmarking against the theoretical limit. *ACS Energy Lett* 2023;8:981–7.
- [12] Liang H, Han H, Wang F, Cheng Z, Lin B, Pan Y, et al. Experimental investigation on spectral splitting of photovoltaic/thermal hybrid system with two-axis sun tracking based on SiO₂/TiO₂ interference thin film. *Energy Convers Manag* 2019;188:230–40.
- [13] Dai H, Jiang B, Hu X, Lin X, Wei X, Pecht M. Advanced battery management strategies for a sustainable energy future: multilayer design concepts and research trends. *Renew Sustain Energy Rev* 2021;138:110480.
- [14] Piraram A, Talebzadeh N, Leung SN, O'Brien PG. Radiative cooling for buildings: a review of techno-enviro-economics and life-cycle assessment methods. *Renew Sustain Energy Rev* 2022;162:112415.
- [15] Ruan ZH, Gao P, Yuan Y, Tan HP. Theoretical estimation of temperature-dependent radiation properties of molten solar salt using molecular dynamics and first principles. *Energy* 2022;246:123379.
- [16] Zhang P, Qiu Y, Ye C, Li Q. Anisotropically conductive phase change composites enabled by aligned continuous carbon fibers for full-spectrum solar thermal energy harvesting. *Chem Eng J* 2023;141940.
- [17] Dong Y, Wang F, Zhang Y, Shi X, Zhang A, Shuai Y. Experimental and numerical study on flow characteristic and thermal performance of macro-capsules phase change material with biomimetic oval structure. *Energy* 2022;238:121830.
- [18] Wang K, Zhang ZD, Zhang XY, Min CH. Buoyancy effects on convective heat transfer of supercritical CO₂ and thermal stress in parabolic trough receivers under non-uniform solar flux distribution. *Int J Heat Mass Tran* 2021;175:121130.
- [19] Hossain MM, Gu M. Radiative cooling: principles, progress, and potentials. *Adv Sci* 2016;3:1500360.
- [20] Liu J, Tang H, Jiang C, Wu S, Ye L, Zhao D, et al. Micro-nano porous structure for efficient daytime radiative sky cooling. *Adv Funct Mater* 2022;32:2206962.
- [21] Bellos E, Iliadis P, Papalexis C, Rotas R, Nikolopoulos N, Kosmatopoulos E, Halmidienst C. Dynamic investigation of centralized and decentralized storage systems for a district heating network. *J Energy Storage* 2022;56:106072.
- [22] Wang S, Zhou Y, Jiang T, Yang R, Tan G, Long Y. Thermochromic smart windows with highly regulated radiative cooling and solar transmission. *Nano Energy* 2021;89:106440.
- [23] Xue X, Qiu M, Li Y, Zhang QM, Li S, Yang Z, et al. Creating an eco-friendly building coating with smart subambient radiative cooling. *Adv Mater* 2020;32:1906751.
- [24] Fan S, Li W. Photonics and thermodynamics concepts in radiative cooling. *Nat Photonics* 2022;16:182–90.
- [25] Zhao B, Liu J, Hu M, Ao X, Li L, Xuan Q, et al. Performance analysis of a broadband selective absorber/emitter for hybrid utilization of solar thermal and radiative cooling. *Renew Energy* 2023;205:763–71.
- [26] Liu J, Zhang Y, Li C, Valenzuela C, Shi S, Jiang C, et al. Emerging materials and engineering strategies for performance advance of radiative sky cooling technology. *Chem Eng J* 2023;453:139739.
- [27] Yin X, Yang R, Tan G, Fan S. Terrestrial radiative cooling: using the cold universe as a renewable and sustainable energy source. *Science* 2020;370:786–91.
- [28] Chen Y, Mandal J, Li W, Smith-Washington A, Tsai CC, Huang W, et al. Colored and paintable bilayer coatings with high solar-infrared reflectance for efficient cooling. *Sci Adv* 2020;6: eaaz5413.
- [29] Hu M, Zhao B, Suhendri S, Cao J, Wang Q, Riddat S, et al. Experimental study on a hybrid solar photothermal and radiative cooling collector equipped with a rotatable absorber/emitter plate. *Appl Energy* 2022;306:118096.
- [30] Wu SL, Cao YJ, Li YQ, Sun W. Recent Advances in material engineering and applications for passive daytime radiative cooling. *Adv Opt Mater* 2022;11:2202163.
- [31] Deppe T, Munday NM. Nighttime photovoltaic cells: electrical power generation by optically coupling with deep space. *ACS Photonics* 2020;7(1):1–9.
- [32] Zhai H, Fan D, Li Q. Dynamic radiation regulations for thermal comfort. *Nano Energy* 2022;100:107435.
- [33] Li Y, Chen X, Li Y, Pang D, Yan H, Chen M. Janus-interface engineering boosting visibly transparent radiative cooling for energy-saving. *ACS Appl Mater Interfaces* 2023;15:4122–31.
- [34] Zhang J, Zhou Z, Quan J, Zhang D, Sui J, Yu J, et al. A flexible film to block solar radiation for daytime radiative cooling. *Sol Energy Mater Sol Cells* 2021;225:111029.
- [35] Wang F, Cheng Z, Tan J, Yuan Y, Shuai Y, Liu L. Progress in concentrated solar power technology with parabolic trough collector system: a comprehensive review. *Renew Sustain Energy Rev* 2017;79:1314–28.
- [36] Bao H, Yan C, Wang B, Fang X, Zhao CY, Ruan X. Double-layer nanoparticle-based coatings for efficient terrestrial radiative cooling. *Sol Energy Mater Sol Cells* 2017;168:78–84.
- [37] Li M, Coimbra CFM. On the effective spectral emissivity of clear skies and the radiative cooling potential of selectively designed materials. *Int J Heat Mass Tran* 2019;135:1053–62.
- [38] Baranov DG, Xiao Y, Nechepurenko IA, Krasnok A, Alù A, Kats MA. Nanophotonic engineering of far-field thermal emitters. *Nat Mater* 2019;18:920–30.
- [39] Zhao B, Lu K, Hu M, Wang K, Gao D, Chen K, et al. Sub-ambient daytime radiative cooling based on continuous sunlight blocking. *Sol Energy Mater Sol Cells* 2022;321:119357.
- [40] Wang J, Tan G, Yang R, Zhao D. Materials, structures, and devices for dynamic radiative cooling. *Cell Rep Phys Sci* 2022;3:101198.
- [41] Chen M, Pang D, Chen X, Yan H, Yang Y. Passive daytime radiative cooling: fundamentals, material designs, and applications. *EcoMat* 2021;4:e12153.
- [42] Yu X, Chan J, Chen C. Review of radiative cooling materials: performance evaluation and design approaches. *Nano Energy* 2021;88:106259.
- [43] Lin C, Li Y, Chi C, Kwon YS, Huang J, Wu Z, et al. A solution-processed inorganic emitter with high spectral selectivity for efficient subambient radiative cooling in hot humid climates. *Adv Mater* 2022;34:2109350.
- [44] Gentle AR, Smith GB. Radiative heat pumping from the earth using surface phonon resonant nanoparticles. *Nano Lett* 2010;10:373–9.
- [45] Fang H, Xie W, Li X, Fan K, Lai YT, Sun B, et al. A triple-mode midinfrared modulator for radiative heat management of objects with various emissivity. *Nano Lett* 2021;21:4106–14.
- [46] Chen G, Wang Y, Qiu J, Cao J, Zou Y, Wang S, et al. Robust inorganic daytime radiative cooling coating based on a phosphate geopolymers. *ACS Appl Mater Interfaces* 2020;12:54963–71.
- [47] Zhang H, Huang J, Fan D. Switchable radiative cooling from temperature-responsive thermal resistance modulation. *ACS Appl Energy Mater* 2022;5:6003–10.
- [48] Wang X, Liu X, Li Z, Zhang H, Yang Z, Zhou H, et al. Scalable flexible hybrid membranes with photonic structures for daytime radiative cooling. *Adv Funct Mater* 2020;30:1907562.
- [49] Zhang X, Yang L, Wang F, Cheng Z, Liang H. Wrinkled surface microstructure for enhancing the infrared spectral performance of radiative cooling. *Opt Express* 2021;29:11416–32.
- [50] Lin KT, Han J, Li K, Guo C, Lin H, Jia B. Radiative cooling: fundamental physics, atmospheric influences, materials and structural engineering, applications and beyond. *Nano Energy* 2021;80:105517.
- [51] Liang H, Wang F, Li D, Zhu J, Tan J. Optical properties and transmittances of ZnO-containing nanofluids in spectral splitting photovoltaic/thermal systems. *Int J Heat Mass Tran* 2019;128:668–78.
- [52] Donahue RJ, Foster DE. Effects of oxygen enhancement on the emissions from a di diesels via manipulation of fuels and combustion chamber gas composition. Society of Automotive Engineers; 2000.
- [53] Dong M, Zhu L, Jiang B, Fan S, Chen Z, Chen Z, Yan H. Concentrated radiative cooling and its constraint from reciprocity. *Opt Express* 2022;30:275–85.
- [54] Zhao Y, Pang D, Chen M, Chen Z, Yan H. Scalable aqueous processing-based radiative cooling coatings for heat dissipation applications. *Appl Mater Today* 2022;26:101298.

- [55] Xu Z, Li N, Liu D, Huang X, Wang J, Wu W, et al. A new crystal $Mg_{11}(HPO_4)_8(OH)_6$ for daytime radiative cooling. *Sol Energy Mater Sol Cells* 2018;185:536–41.
- [56] Chen M, Pang D, Yan H. Sustainable and self-cleaning bilayer coatings for high-efficient daytime radiative cooling. *J Mater Chem C* 2022;10:8329–38.
- [57] Yun J, Chae D, So S, Lim H, Noh J, Park J, et al. Optimally Designed multimaterial microparticle–polymer composite paints for passive daytime radiative cooling. *ACS Photonics* 2023;10:2608–17.
- [58] Guan Q, Raza A, Mao SS, Vega LF, Zhang T. Machine learning-enabled inverse design of radiative cooling film with on-demand transmissive color. *ACS Photonics* 2023;10:715–26.
- [59] Chen Q, Lu Y, Zhang J, Li D, Huang T, Lou C, et al. Flexible structural polyethylene films for dynamically tunable energy harvesting from the sun and outer space. *Nano Energy* 2023;114:108610.
- [60] Su W, Cai P, Darkwa J, Hu M, Kokogiannakis G, Xu C, et al. Review of daytime radiative cooling technologies and control methods. *Appl Therm Eng* 2023;235:121305.
- [61] Chen M, Pang D, Mandal J, Chen X, Yan H, He Y, et al. Designing mesoporous photonic structures for high-performance passive daytime radiative cooling. *Nano Lett* 2021;21:1412–8.
- [62] Ma LX, Tan JY, Zhao JM, Wang FQ, Wang CA. Multiple and dependent scattering by densely packed discrete spheres: comparison of radiative transfer and Maxwell theory. *J Quant Spectrosc Radiat Transf* 2017;187:255–66.
- [63] Bijarni JP, Sarkar J, Maiti P. Review on passive daytime radiative cooling: fundamentals, recent researches, challenges and opportunities. *Renew Sustain Energy Rev* 2020;133:110263.
- [64] Venumbaka MR, Raina JP, Marepally BC. Plasmonic E-field enhancements and coupling effects of metallic structures using FDTD. *Mater Today Proc* 2021;47:1855–61.
- [65] Sullivan DM. Electromagnetic simulation using the FDTD method. IEEE Press; 2000.
- [66] Wang CH, Liu MX, Jiang ZY. TiO_2 particle agglomeration impacts on radiative cooling films with a thickness of 50 μm . *Appl Phys Lett* 2022;121:202204.
- [67] Cheng Z, Wang F, Gong D, Liang H, Shuai Y. Low-cost radiative cooling blade coating with ultrahigh visible light transmittance and emission within an ‘atmospheric window’. *Sol Energy Mater Sol Cells* 2020;213:110563.
- [68] Luo M, Zhao J, Liu L. Heat diffusion in nanoparticle systems via near-field thermal photons. *Int J Heat Mass Tran* 2023;200:123544.
- [69] Ma LX, Xie BW, Wang CC, Liu LH. Radiative transfer in dispersed media: considering the effect of host medium absorption on particle scattering. *J Quant Spectrosc Radiat Transf* 2019;203:24–35.
- [70] Ma LX, Wang FQ, Wang CH, Wang CC, Tan JY. Investigation of the spectral reflectance and bidirectional reflectance distribution function of sea foam layer by the Monte Carlo method. *Appl Opt* 2015;54:9863–74.
- [71] Ma L, Wang C, Liu L. Polarized radiative transfer in dense dispersed media containing optically soft sticky particles. *Opt Express* 2020;28:28252–68.
- [72] Zhang A, Wang F, Dong Y, Yang D, Xie W. Dependent scattering criterion modification of disordered dispersed particulate medium with the consideration of particle random distribution and high complex refractive index effects. *Int J Heat Mass Tran* 2022;197:123331.
- [73] Huang W, Chen Y, Luo Y, Mandal J, Li W, Chen M, et al. Scalable aqueous processing-based passive daytime radiative cooling coatings. *Adv Funct Mater* 2021;31:2010334.
- [74] Cheng Z, Lin B, Shi X, Wang F, Ling H, Shuai Y. Influences of atmospheric water vapor on spectral effective emissivity of a single-layer radiative cooling coating. *AIMS Energy* 2021;9:96–116.
- [75] Gao Y, Song X, Farooq AS, Zhang P. Cooling performance of porous polymer radiative coating under different environmental conditions throughout all-year. *Sol Energy* 2021;228:474–85.
- [76] Cheng ZM, Shuai Y, Gong DY, Wang FQ, Liang HX, Li GQ. Optical properties and cooling performance analyses of single-layer radiative cooling coating with mixture of TiO_2 particles and SiO_2 particles. *Sci China Technol Sci* 2021;64:1017–29.
- [77] Cheng Z, Wang F, Wang H, Liang H, Ma L. Effect of embedded polydisperse glass microspheres on radiative cooling of a coating. *Int J Therm Sci* 2019;140:358–67.
- [78] Wang F, Wang H, Gong D, Cheng Z, Ma L. Radiative transfer analysis of semitransparent medium with particles having non-uniform size distribution by differential-integration method. *Int J Heat Mass Tran* 2019;130:342–55.
- [79] Wang F, Ma L, Cheng Z, Tan J, Xuang X, Liu L. Radiative heat transfer in solar thermochemical particle reactor: a comprehensive review. *Renew Sustain Energy Rev* 2017;73:935–49.
- [80] Ma LX, Tan JY, Zhao JM, Wang FQ, Wang CA, Wang YY. Dependent scattering and absorption by densely packed discrete spherical particles: effects of complex refractive index. *J Quant Spectrosc Radiat Transf* 2017;196:94–102.
- [81] Tan J, Xie Y, Wang F, Jing L, Ma L. Investigation of optical properties and radiative transfer of TiO_2 nanofluids with the consideration of scattering effects. *Int J Heat Mass Tran* 2017;115:1103–12.
- [82] Xu J, Wan R, Xu W, Ma Z, Cheng X, Yang R, et al. Colored radiative cooling coatings using phosphor dyes. *Mater Today Nano* 2022;19:100239.
- [83] Dong Y, Han H, Wang F, Zhang Y, Cheng Z, Shi X, et al. A low-cost sustainable coating: improving passive daytime radiative cooling performance using the spectral band complementarity method. *Renew Energy* 2022;192:606–16.
- [84] Wang F, Zhang X, Wang H, Li Y, Dong Y, Lin B, et al. An energy-efficient glass using biomimetic structures with excellent energy saving features in both hot and cold weather. *J Quant Spectrosc Radiat Transf* 2022;286:108180.
- [85] Zhou K, Li W, Patel BB, Tao R, Chang Y, Fan S, et al. Three-dimensional printable nanoporous polymer matrix composites for daytime radiative cooling. *Nano Lett* 2021;21:1493–9.
- [86] https://www.freepik.com/free-photo/autumn-leaf-covered-with-ice-crystals-early-morning-cold-season_11913002.htm. [Accessed 14 February 2023].
- [87] <https://physicsworld.com/wp-content/uploads/2016/04/PW-2016-04-18-silver-ants.jpg>. [Accessed 14 February 2023].
- [88] <https://news.un.org/zh/story/2022/12/1113507>. [Accessed 20 August 2023].
- [89] Tadepalli S, Slocik JM, Gupta MK, Naik RR, Singamaneni S. Bio-optics and bio-inspired optical materials. *Chem Rev* 2017;117:12705–63.
- [90] Tian Y, Liu X, Zheng H, Xu Q, Zhu Z, Luo Q. Artificial mitochondrion for fast latent heat storage: experimental study and lattice Boltzmann simulation. *Energy* 2022;245:123296.
- [91] Wang F, Zhang G, Shi X, Dong Y, Xun Y, Zhang A. Biomimetically calabash-inspired phase change material capsule: experimental and numerical analysis on thermal performance and flow characteristics. *J Energy Storage* 2022;52:104859.
- [92] Liu X, Chen M, Xu Q, Gao K, Fang C, Li P. Bamboo derived SiC ceramics-phase change composites for efficient, rapid, and compact solar thermal energy storage. *Sol Energy Mater Sol Cells* 2022;240:111726.
- [93] Liu F, Wang J, Liu Y, Wang F, Yang N, Liu X. Performance analysis of phase change material in battery thermal management with biomimetic honeycomb fin. *Appl Therm Eng* 2021;196:117296.
- [94] Yang J, Zhang X, Zhang X, Wang L, Feng W, Li Q. Beyond the visible: bioinspired infrared adaptive materials. *Adv Mater* 2021;33:2004754.
- [95] Zhang X, Shi X, Li Y, Wang F, Lin B. Biomimetic hierarchical structure for enhancing concentrated solar energy converting and utilizing efficiency. *Opt Express* 2021;29:26669–84.
- [96] Shi NN, Tsai CC, Camino F, Bernard GD, Yu N, Wehner R. Keeping cool: enhanced optical reflection and radiative heat dissipation in Saharan silver ants. *Science* 2015;349:298–301.
- [97] Wang S, Wang Y, Zou Y, Chen G, Ouyang J, Jia D, et al. Biologically inspired scalable-manufactured dual-layer coating with a hierarchical micropattern for highly efficient passive radiative cooling and robust superhydrophobicity. *ACS Appl Mater Interfaces* 2021;13:21888–97.
- [98] Mitchell D, Henschel JR, Hetem RS, Wassenaar TD, Strauss WM, Hanrahan SA, et al. Fog and fauna of the Namib Desert: past and future. *Ecosphere* 2020;11:e02996.
- [99] Feng J, Gao K, Jiang Y, Ulpiani G, Krajcic D, Paolini R, et al. Optimization of random silica-polymethylpentene (TPX) radiative coolers towards substantial cooling capacity. *Sol Energy Mater Sol Cells* 2022;234:111419.
- [100] Cai C, Chen W, Wei Z, Ding C, Sun B, Gerhard C, et al. Bioinspired “aerogel grating” with metasurfaces for durable daytime radiative cooling for year-round energy savings. *Nano Energy* 2023;114:108625.
- [101] Li S, Xu D, Zhao J, Liu L. Random rough surface effects on the performance of near-field thermophotovoltaic system. *Int J Heat Mass Tran* 2023;202:123713.
- [102] Cheng Z, Han H, Wang F, Yan Y, Shi X, Liang H, et al. Efficient radiative cooling coating with biomimetic human skin wrinkle structure. *Nano Energy* 2021;89:106377.
- [103] https://glossary.ametsoc.org/wiki/Radiation_fog. [Accessed 14 February 2023].
- [104] Zheng S, Shi Y, Wang Z, Wang P, Liu G, Zhou H. Development of new technology for coal gasification purification and research on the formation mechanism of pollutants. *Int J Coal Sci Techn* 2021;8:335–48.
- [105] <https://www.birdsoutsidemywindow.org/2012/10/24/radiation-fog/>. [Accessed 14 February 2023].
- [106] <https://resources.eumetrain.org/data/2/24/Content/theory1.htm>. [Accessed 14 February 2023].
- [107] Zheng S, Liu H, He Y, Yang Y, Sui R, Lu Qiang. Combustion of biomass pyrolysis gas: roles of radiation reabsorption and water content. *Renew Energy* 2023;205:864–72.
- [108] Lakra K, Avishhek K. A review on factors influencing fog formation, classification, forecasting, detection and impacts. *Rendiconti Lincei Sci Fis Nat* 2022;33:319–53.
- [109] Gultepe I, Zhou B, Milbrandt J, Bott A, Li Y, Heymsfield AJ, et al. A review on ice fog measurements and modeling. *Atmos Res* 2015;151:2–19.
- [110] [https://commons.wikimedia.org/wiki/File:Радиационна_Магла_1.jpg/](https://commons.wikimedia.org/wiki/File:Радиационна_Магла_1.jpg). [Accessed 20 August 2023].
- [111] Chen M, Pang D, Chen X, Yan H. Enhancing infrared emission behavior of polymer coatings for radiative cooling applications. *J Phys D Appl Phys* 2021;54:295501.
- [112] Li N, Wang J, Liu D, Huang X, Xu Z, Zhang C, et al. Selective spectral optical properties and structure of aluminum phosphate for daytime passive radiative cooling application. *Sol Energy Mater Sol Cells* 2019;194:103–10.
- [113] Chen M, Pang D, Yan H. Infrared transparent passive daytime radiative cooling for non-contact heat dissipations. *iScience* 2022;25:104726.
- [114] Li T, Zhai Y, He S, Gan W, Wei Z, Heidarinejad M. A radiative cooling structural material. *Science* 2019;364:760–3.
- [115] Aili A, Wei ZY, Chen YZ, Zhao DL, Yang RG, Yin XB. Selection of polymers with functional groups for daytime radiative cooling. *Mater Today Phys* 2019;10:100127.
- [116] Zhou Z, Wang X, Ma Y, Hu B, Zhou J. Transparent polymer coatings for energy-efficient daytime window cooling. *Cell Rep Phys Sci* 2020;1:100231.
- [117] Anderson RJ, Bendell DJ, Groundwater PW. Organic spectroscopic analysis. Royal Society of Chemistry; 2004.
- [118] Stuart BH. Infrared spectroscopy: Fundamentals and applications. J Wiley; 2004.
- [119] Wang T, Wu Y, Shi L, Hu X, Chen M, Wu L. A structural polymer for highly efficient all-day passive radiative cooling. *Nat Commun* 2021;12:365.

- [120] Zeng S, Pian S, Su M, Wang Z, Wu M, Liu X, et al. Hierarchical-morphology metafabric for scalable passive daytime radiative cooling. *Science* 2021;373:693–6.
- [121] Liu L, Zhang H, Cai Y, Li Y, Qin J, Yang Z, et al. Super-amphiphobic coatings with sub-ambient daytime radiative cooling—Part 2: cooling effect under real conditions. *Sol Energy Mater Sol Cells* 2022;241:111736.
- [122] Chen S, Lin K, Pan A, Ho TC, Zhu Y, Tso CY. Study of a passive radiative cooling coating on chemical storage tanks for evaporative loss control. *Renew Energy* 2023;211:326–35.
- [123] Yue Q, Zhang L, He CY, Liu BH, Wang WM, Lu ZW. Polymer composites with hierarchical architecture and dielectric particles for efficient daytime subambient radiative cooling. *J Mater Chem A* 2023;11:3126–35.
- [124] Li X, Peoples J, Yao P, Ruan X. Ultrawhite BaSO₄ Paints and films for remarkable daytime subambient radiative cooling. *ACS Appl Mater Interfaces* 2021;13:21733–9.
- [125] Li X, Peoples J, Huang Z, Zhao Z, Qiu J, Run X. Full daytime sub-ambient radiative cooling in commercial-like paints with high figure of merit. *Cell Rep Phys Sci* 2020;1:100221.
- [126] Li M, Liao Z, Coimbra CFM. Spectral model for clear sky atmospheric longwave radiation. *J Quant Spectrosc Radiat Transf* 2018;209:196–211.
- [127] Chen S, Liang Z, Dong P, Guo S, Li M. A transferable turbidity estimation method for estimating clear-sky solar irradiance. *Renew Energy* 2023;206:633–44.
- [128] Li D, Liu X, Li W, Lin Z, Zhu B, Li Z, et al. Scalable and hierarchically designed polymer film as a selective thermal emitter for high-performance all-day radiative cooling. *Nat Nanotechnol* 2021;16:153–8.
- [129] Li P, Wang A, Fan J, Kang Q, Jiang P, Bao H, et al. Thermo-optically designed scalable photonic films with high thermal conductivity for subambient and above-ambient radiative cooling. *Adv Funct Mater* 2022;32:2109542.
- [130] Liang H, Wang F, Cheng Z, Hu S, Xiao B, Gong X, et al. Analyzing the effects of reaction temperature on photo-thermo chemical synergistic catalytic water splitting under full-spectrum solar irradiation: an experimental and thermodynamic investigation. *Int J Hydrogen Energy* 2017;42:12133–42.
- [131] Luo H, Yang M, Guo J, Zou W, Xu J, Zhao N. Hierarchical porous polymer coatings based on uv-curing for highly efficient passive all-day radiative cooling. *ACS Appl Polym Mater* 2022;4:5746–55.
- [132] Song J, Zhang W, Sun Z, Pan M, Tian Fm Ku X, et al. Durable radiative cooling against environmental aging. *Nat Commun* 2022;13:4805.
- [133] Dong Y, Zou Y, Li X, Wang F, Cheng Z, Meng W, et al. Introducing masking layer for daytime radiative cooling coating to realize high optical performance, thin thickness, and excellent durability in long-term outdoor application. *Appl Energy* 2023;344:121273.
- [134] Peoples J, Li X, Lv Y, Qiu J, Huang Z, Ruan X. A strategy of hierarchical particle sizes in nanoparticle composite for enhancing solar reflection. *Int J Heat Mass Tran* 2019;131:487–94.
- [135] Liang H, Wang F, Cheng Z, Xu C, Li G, Shuai Y. Full-spectrum solar energy utilization and enhanced solar energy harvesting via photon anti-reflection and scattering performance using biomimetic nanophotonic structure. *ES Energy & Environment* 2020;8:29–41.
- [136] Liang H, Wang F, Cheng Z, Shi X, Han H. Reducing toxicity and enhancing broadband solar energy harvesting of ultra-thin perovskite solar cell via SiO₂ nanophotonic structure. *Optik* 2020;223:165624.
- [137] Liu J, Xu C, Ao X, Lu K, Zhao B, Pei G. A dual-layer polymer-based film for all-day sub-ambient radiative sky cooling. *Energy* 2022;256:124350.
- [138] Meng S, Long L, Wu Z, Deniski N, Yang Y, Wang L, et al. Scalable dual-layer film with broadband infrared emission for sub-ambient daytime radiative cooling. *Sol Energy Mater Sol Cells* 2020;208:110393.
- [139] Wang N, Lv Y, Zhao D, Zhao W, Xu J, Yang R. Performance evaluation of radiative cooling for commercial-scale warehouse. *Mater Today Energy* 2022;24:100927.
- [140] Ma H, Wang L, Dou S, Zhao H, Huang M, Xu Z, et al. Flexible daytime radiative cooling enhanced by enabling three-phase composites with scattering interfaces between silica microspheres and hierarchical porous coatings. *ACS Appl Mater Interfaces* 2021;13:19282–90.
- [141] Atiganyan S, Plumley JB, Han SJ, Hsu K, Cytrynbaum J, Peng TL, et al. Effective radiative cooling by paint-format microsphere-based photonic random media. *ACS Photonics* 2018;5:1181–7.
- [142] Song J, Cheng Z, Fan Y, Wang F, Shi X, Xu J, et al. Human ear inspired solar thermochemical reactor for steam methane reforming with the consideration of minimum Gibbs free energy principle. *J Energy Storage* 2023;72:108172.
- [143] Shi X, Zhang X, Wang F, Yang L, Dong Y, Shuai Y. Hermochemical analysis of dry methane reforming hydrogen production in biomimetic venous hierarchical porous structure solar reactor for improving energy storage. *Int J Hydrogen Energy* 2021;46:7733–44.
- [144] Liu H, Kang H, Jia X, Qiao X, Qin W, Wu X. Commercial-like self-cleaning colored ZrO₂-based bilayer coating for remarkable daytime sub-ambient radiative cooling. *Adv Mater Technol* 2022;7:2101583.
- [145] Zou Y, Li X, Yang L, Zhang B, Wu X. Efficient direct absorption solar collector based on hollow TiN nanoparticles. *Int J Therm Sci* 2023;185:108099.
- [146] Han D, Fei J, Mandal J, Liu Z, Li H, Raman AP, et al. Sub-ambient radiative cooling under tropical climate using highly reflective polymeric coating. *Sol Energy Mater Sol Cells* 2022;240:111723.
- [147] Zou C, Ren G, Hossain MM, Nirantar S, Withayachumankul W, Ahmed T, et al. Metal-loaded dielectric resonator metasurfaces for radiative cooling. *Adv Opt Mater* 2017;5:1700460.
- [148] Sun K, Ridedl CA, Wang Y, Urban A, Simeoni M, Zalkovskij M, et al. Metasurface optical solar reflectors using AZO transparent conducting oxides for radiative cooling of spacecraft. *ACS Photonics* 2018;5:495–501.
- [149] Jeon S, Son S, Min S, Park H, Lee H, Shin J. Daylong sub-ambient radiative cooling with full-color exterior based on thermal radiation and solar decoupling. *Adv Opt Mater* 2023;11:2202129.
- [150] Rephaeli E, Raman A, Fan S. Ultrabroadband photonic structures to achieve high-performance daytime radiative cooling. *Nano Lett* 2013;13:1457–61.
- [151] Xu HJ, Xing ZB, Wang FQ, Cheng ZM. Review on heat conduction, heat convection, thermal radiation and phase change heat transfer of nanofluids in porous media: fundamentals and applications. *Chem Eng Sci* 2019;195:462–83.
- [152] Lee D, Go M, Son S, Kim M, Badloe T, Lee H, et al. Sub-ambient daytime radiative cooling by silica-coated porous anodic aluminum oxide. *Nano Energy* 2021;79:105426.
- [153] Wang F, Shuai Y, Tan H, Yu C. Thermal performance analysis of porous media receiver with concentrated solar irradiation. *Int J Heat Mass Tran* 2013;62:247–54.
- [154] Fei J, Han D, Ge J, Wang X, Koh SW, Gao S, et al. Switchable surface coating for bifunctional passive radiative cooling and solar heating. *Adv Funct Mater* 2022;32:2203582.
- [155] Zhang WB, Wang BX, Xu JM, Zhao CY. High-quality quasi-monochromatic near-field radiative heat transfer designed by adaptive hybrid Bayesian optimization. *Sci China Technol Sci* 2022;65:2910–20.
- [156] Zhang X, Li X, Wang F, Yuan W, Cheng Z, Liang H. Low-cost and large-scale producible biomimetic radiative cooling glass with multiband radiative regulation performance. *Adv Opt Mater* 2022;10:2202031.
- [157] Jin S, Yi F, Xu J, Wang B, Zhao C. Planar coupled nanocavities for efficient solar spectrum engineering. *Adv Opt Mater* 2023;23000980.
- [158] Xie B, Zhang W, Zhao J, Liu L. VO₂-based superposed Fabry-Perot multilayer film with a highly enhanced infrared emittance and emittance tunability for spacecraft thermal control. *Opt Express* 2022;30:34314–27.
- [159] Ma H, Yao K, Dou S, Xiao M, Dai M, Wang L, et al. Multilayered SiO₂/Si₃N₄ photonic emitter to achieve high-performance all-day radiative cooling. *Sol Energy Mater Sol Cells* 2020;212:110584.
- [160] Jin S, Xiao M, Zhang W, Wang B, Zhao C. Daytime sub-ambient radiative cooling with vivid structural colors mediated by coupled nanocavities. *ACS Appl Mater Interfaces* 2022;14:54676–87.
- [161] Jin SH, Xiao M, Chen J, Xu JM, Wang BX, Zhao CY. Nanocomposite coatings with plasmonic structural colors for subambient daytime radiative cooling. *Sol Energy* 2022;240:211–24.
- [162] Chen M, Pang D, Yan H. Colored passive daytime radiative cooling coatings based on dielectric and plasmonic spheres. *Appl Therm Eng* 2022;216:119125.
- [163] Yu S, Chen J, Gomard G, Hölscher H, Lemmer U. Recent progress in light-scattering porous polymers and their applications. *Adv Opt Mater* 2023;11:2203134. AOM.
- [164] Liu J, Zhang D, Jiao S, Zhou Z, Zhang Z, Gao F. Daytime radiative cooling with clear epoxy resin. *Sol Energy Mater Sol Cells* 2020;207:110368.
- [165] Zhang A, Wang F, Cheng Z, Liang H, Shi X. Radiative property investigation of dispersed particulate medium with the consideration of non-uniform particle size distribution and dependent scattering effects. *Int J Heat Mass Tran* 2022;186:122488.
- [166] Fu ZC, Cheng ZM, Wang FQ, Dong Y, Zhang XP, Zhang AY, et al. A multilayer film based on thin-film interference and impedance matching for dual-laser and infrared stealth as well as thermal management. *Optik* 2023;289:171261.
- [167] Zhang A, Cheng Z, Wang F, Xie W, Liang H. Radiative property investigation of metal nanoparticles embedded in absorption layer for thin-film solar cell with the consideration of medium absorption and dependent scattering. *Opt Commun* 2023;545:129654.
- [168] Chen M, Li S, Pang D, Zhao Y, Yang Y, Yan H. Numerically enhancing daytime radiative cooling performance of random dielectric microsphere coatings by hollow structures. *J Photon Energy* 2021;11:042108.
- [169] Sun J, Wang J, Guo T, Bao H, Bai S. Daytime passive radiative cooling materials based on disordered media: a review. *Sol Energy Mater Sol Cells* 2022;236:111492.
- [170] Cheng Z, Wang F, Liang H, Hu S, Lin B, Tan J. Photon-absorption-based explanation of ultrasonic-assisted solar photochemical splitting of water to improve hydrogen production. *Int J Hydrogen Energy* 2018;43:14439–50.
- [171] Zhai Y, Ma Y, David SN, Zhao D, Luo R, Tan G, et al. Scalable-manufactured randomized glass-polymer hybrid metamaterial for daytime radiative cooling. *Science* 2017;355:1062–6.
- [172] Huang Z, Ruan X. Nanoparticle embedded double-layer coating for daytime radiative cooling. *Int J Heat Mass Tran* 2017;104:890–6.
- [173] Zhou K, Yan X, Oh SJ, Padila-Rivera Gabriela, Kim HA, Cropek DM, et al. Hierarchically patterned self-cleaning polymer composites for daytime radiative cooling. *Nano Lett* 2023;23:3669–77.
- [174] Cai C, Wei Z, Ding C, Sun B, Chen W, Gerhard C, Nimerovsky E, et al. Dynamically tunable all-weather daytime cellulose aerogel radiative supercooler for energy-saving building. *Nano Lett* 2022;22:4106–14.
- [175] Akerboom E, Veeken T, Hecker C, Groep Jvd, Polman A. Passive radiative cooling of silicon solar modules with photonic silica microcylinders. *ACS Photonics* 2022;9:3831–40.
- [176] Yu S, Zhang Q, Wang Y, Lv Y, Ma R. Photonic-structure colored radiative coolers for daytime subambient cooling. *Nano Lett* 2022;22:4925–32.
- [177] Feng S, Zhou Y, Chen X, Shi S, Liu C, Zhang T. Bio-skin inspired 3D porous cellulose/AlPO₄ nano-laminated film with structure-enhanced selective emission for all-day non-power cooling. *J Mater Chem A* 2021;9:25178–88.
- [178] Chang X, Cheng Z, Yang D, Dong Y, Shi X, Liang H, et al. Scalable bio-skin-inspired radiative cooling metafabric for breaking trade-off between optical properties and application requirements. *ACS Photonics* 2023;10:1624–32.

- [179] Guo L, Fan D, Li Q. Variable emittance behavior of smart radiative coating. *Mater Res Express* 2016;3:025008.
- [180] Xie D, Wang Z, Liu X, Cui S, Zhou H, Fan T. Broadband omnidirectional light reflection and radiative heat dissipation in white beetles *Goliathus goliatus*. *Soft Matter* 2019;15:4294–300.
- [181] Zhang H, Ly KCS, Liu X, Chen Z, Yan M, Wu Z, et al. Biologically inspired flexible photonic films for efficient passive radiative cooling. *Proc Natl Acad Sci USA* 2020;117:14657–66.
- [182] Wang F, Zhang X, Dong Y, Yi H, Shi X, Li Y. Progress in radiative transfer in porous medium: a review from macro scale to pore scale with experimental test. *Appl Therm Eng* 2022;210:118331.
- [183] Chen X, Wang F, Han Y, Yu R, Cheng Z. Thermochemical storage analysis of the dry reforming of methane in foam solar reactor. *Energy Convers Manag* 2018;158: 489–98.
- [184] Zhou L, Zhao J, Huang H, Nan F, Zhou G, Ou Q. Flexible polymer photonic films with embedded microvoids for high-performance passive daytime radiative cooling. *ACS Photonics* 2021;8:3301–7.
- [185] Luo M, Wang C, Zhao J, Liu L. Characteristics of effective thermal conductivity of porous materials considering thermal radiation: a pore-level analysis. *Int J Heat Mass Tran* 2022;188:122597.
- [186] Mandal J, Fu Y, Overvig A, Jia M, Sun K, Shi N, et al. Hierarchically porous polymer coatings for highly efficient passive daytime radiative cooling. *Science* 2018;362:315–9.
- [187] Chen M, Li S, Pang D, Yang Y, Yan H. Enhanced radiative cooling performance of randomly dielectric microsphere coatings using hollow structure. *J Photon Energy* 2021;11:042108.
- [188] Huang J, Fan D, Li Q. Structural rod-like particles for highly efficient radiative cooling. *Mater Today Energy* 2022;25:100955.
- [189] Huang J, Li M, Fan D. Core-shell particles for devising high-performance full-day radiative cooling paint. *Appl Mater Today* 2021;25:101209.
- [190] Chen M, Pang D, Chen X, Yan H. Numerically investigating the effective radiative cooling performance of randomly dielectric microsphere coating. *Int J Heat Mass Tran* 2021;173:121263.
- [191] Gao Y, Song X, Zhang P. Comprehensive evaluation and analysis of a porous polymer coating for highly efficient passive radiative cooling. *Sol Energy Mater Sol Cells* 2023;250:112081.
- [192] Liu X, Xiao C, Wang P, Yan M, Wang H, Xie P, et al. Biomimetic photonic multiform composite for high-performance radiative cooling. *Adv Opt Mater* 2021;9:2101151.
- [193] Xiang B, Zhang P, Luo Y, Zhang S, Xu L, Min H, et al. 3D porous polymer film with designed pore architecture and auto-deposited SiO₂ for highly efficient passive radiative cooling. *Nano Energy* 2021;81:105600.
- [194] <https://www.fieldstudyoftheworld.com/persian-ice-house-how-make-ic-e-desert/>. [Accessed 14 February 2023].
- [195] Jing W, Zhang S, Zhang W, Chen Z, Zhang C, Wu D, et al. Scalable and flexible electrospun film for daytime subambient radiative cooling. *ACS Appl Mater Interfaces* 2021;13:29558–66.
- [196] http://ghoolabad.com/index2.asp?cat=d&id=24&charset=kaf_ye. [Accessed 14 February 2023].
- [197] Li J, Liang Y, Li W, Xu N, Zhu B, Wu Z, et al. Protecting ice from melting under sunlight via radiative cooling. *Sci Adv* 2022;8:eabj9756.
- [198] Hu M, Zhao B, Suhendri, Cao J, Wang Q, Riffat S, et al. Effect of vacuum scheme on radiative sky cooling performance. *Appl Therm Eng* 2023;219:119657.
- [199] Chen Z, Zhu L, Raman A, Fan S. Radiative cooling to deep sub-freezing temperatures through a 24-h day-night cycle. *Nat Commun* 2016;7:13729.
- [200] Zhang C, Shen C, Zhang Y, Zheng K, Pu J, Zhao X, et al. Experimental study of indoor light/thermal environment with spectrally selective windows using ATO nanofluids in winter. *Energy Build* 2022;278:112597.
- [201] Zhang C, Shen C, Wei S, Zhang Y, Sun C. Flexible management of heat/electricity of novel PV/T systems with spectrum regulation by Ag nanofluids. *Energy* 2021; 221:119903.
- [202] Yang M, Zhong H, Li T, Wu B, Wang Z, Sun D. Phase change material enhanced radiative cooler for temperature-adaptive thermal regulation. *ACS Nano* 2023;17 (2):1693–700.
- [203] Hu M, Zhao B, Suhendri, Cao J, Wang Q, Riffat S, et al. Extending the operation of a solar air collector to night-time by integrating radiative sky cooling: a comparative experimental study. *Energy* 2022;251:123983.
- [204] Dong Y, Meng W, Wang F, Han H, Liang H, Xiang Li, et al. Warm in winter and cool in summer: scalable biochameleon inspired temperature-adaptive coating with easy preparation and construction. *Nano Lett* 2023. <https://doi.org/10.1021/acs.nanolett.3c02733>.
- [205] Ao Z, Li B, Zhao B, Hu M, Ren H, Yang H, et al. Self-adaptive integration of photothermal and radiative cooling for continuous energy harvesting from the sun and outer space. *Proc Natl Acad Sci USA* 2022;119:e2120557119.
- [206] Wang J, Shan X, Hu P, Zhang C, Yuan D, Hu X, et al. Bioinspired multilayer structures for energy-free passive heating and thermal regulation in cold environments. *ACS Appl Mater Interfaces* 2022;14:46569–80.
- [207] Li X, Xie W, Sui C, Hsu PC. Multispectral thermal management designs for net-zero energy buildings. *ACS Mater Lett* 2020;2:1624–43.
- [208] Mandal J, Yang Y, Yu N, Raman AP. Paints as a scalable and effective radiative cooling technology for buildings. *Joule* 2020;4:1350–6.
- [209] Chen J, Lu L. Comprehensive evaluation of thermal and energy performance of radiative roof cooling in buildings. *J Build Eng* 2021;33:101631.
- [210] Peoples J, Hung YW, Fang Z, Brauna J, Hortob WT, Ruan X. Energy savings of radiative cooling paints applied to residential buildings. *Int J Heat Mass Tran* 2022;194:123001.
- [211] Baniassad A, Sailorb DJ, Ban-Weiss GA. Potential energy and climate benefits of super-cool materials as a rooftop strategy. *Urban Clim* 2019;29:100495.
- [212] Tian D, Zhang J, Gao Z. The advancement of research in cool roof: super cool roof, temperature-adaptive roof and crucial issues of application in cities. *Energy Build* 2023;291:113131.
- [213] Zou H, Wang C, Yu J, Huang D, Yang R, Wang R. Eliminating greenhouse heat stress with transparent radiative cooling film. *Cell Rep Phys Sci* 2023;4:101539.
- [214] Zhai H, Fan D, Li Q. Scalable and paint-format colored coatings for passive radiative cooling. *Sol Energy Mater Sol Cells* 2022;245:111853.
- [215] Zhao D, Aili A, Yin X, Tan G, Yang R. Roof-integrated radiative air-cooling system to achieve cooler attic for building energy saving. *Energy Build* 2019;203:109453.
- [216] Xi Z, Li C, Li Y, Yan H, Chen M. All-day fresh water harvesting by selective solar absorption and radiative cooling. *ACS Appl Mater Interfaces* 2022;14:26255–63.
- [217] Huang X, Mandal J, Xu J, Raman AP. Passive freezing desalination driven by radiative cooling. *Joule* 2022;6:2762–75.
- [218] Li Z, Chen W, Song Y, Zhu B, Zhu J. Fundamentals, materials, and applications for daytime radiative cooling. *Adv Mater Technol* 2020;5:1901007.
- [219] Chen M, Li C, Pang D, Yan H. Selective absorber and emitter boost water evaporation and condensation toward water collection. *Mater Today Energy* 2022;28:101072.
- [220] Chen M, Li S, Yan H. General and scalable fabrication of plasmonic solar selective absorbers by electrodeposition. *Appl Phys Lett* 2023;122:063301.
- [221] Zhou M, Song H, Xu X, Shahsafi A, Xia Z, Ma Z, et al. Vapor condensation with daytime radiative cooling. *Proc Natl Acad Sci USA* 2021;118:e2019292118.
- [222] Yang R, Niu D, Pu JH, Tang GH, Wang X, Du M. Passive all-day freshwater harvesting through a transparent radiative cooling film. *Appl Energy* 2022;325: 119801.
- [223] Zhang Y, Zhu W, Zhang C, Peoples J, Li X, Felicelli AL, et al. Atmospheric water harvesting by large-scale radiative cooling cellulose-based fabric. *Nano Lett* 2022; 22(7):2618–26.
- [224] Haechler I, Park H, Schoenering G, Gulich T, Rohner M, Tripathy A, et al. Exploiting radiative cooling for uninterrupted 24-hour water harvesting from the atmosphere. *Sci Adv* 2021;7:eaab3978.
- [225] Wang Q, Wang F, Wu D, Guo Z. Radiative cooling layer boosting hydrophilic-hydrophobic patterned surface for efficient water harvesting. *Colloid Surf A-Physicochem Eng Asp* 2023;658:130584.
- [226] Chen G, Wang Y, Qiu J, Cao J, Zou Y, Wang S, et al. A facile bioinspired strategy for accelerating water collection enabled by passive radiative cooling and wettability engineering. *Mater Des* 2021;206:109829.
- [227] Amarloo A, Shafii MB. Enhanced solar still condensation by using a radiative cooling system and phase change material. *Desalination* 2019;467:43–50.
- [228] Wang H, Zhang Y, Liang X, Zhang Y. Smart fibers and textiles for personal health management. *ACS Nano* 2021;15:12497–508.
- [229] Cai L, Peng Y, Xu J, Zhou C, Zhou C, Wu P, et al. Temperature regulation in colored infrared-transparent polyethylene textiles. *Joule* 2019;3:1478–86.
- [230] Zhai H, Liu C, Fan D, Li Q. Dual-Encapsulated nanocomposite for efficient thermal buffering in heat-generating radiative cooling. *ACS Appl Mater Interfaces* 2022; 14:57215–24.
- [231] Ma Z, Zhao D, She C, Yang Y, Yang R. Personal thermal management techniques for thermal comfort and building energy saving. *Mater Today Phys* 2021;20: 100465.
- [232] Liu H, Yu J, Zhang S, Ding B. Air-conditioned masks using nanofibrous networks for daytime radiative cooling. *Nano Lett* 2022;22:9485–92.
- [233] Yang A, Cai L, Zhang R, Wang J, Hsu PC, Wang H, et al. Thermal management in nanofiber-based face mask. *Nano Lett* 2017;17:3506–10.
- [234] Miao D, Chen N, Wang X, Yu J, Ding B. Integration of janus wettability and heat conduction in hierarchically designed textiles for all-day personal radiative cooling. *Nano Lett* 2022;22:680–7.
- [235] Zhu B, Li W, Zhang Q, Li D, Liu X, Wang Y, et al. Subambient daytime radiative cooling textile based on nanoprocessed silk. *Nat Nanotechnol* 2021;16:1342–8.
- [236] Xiang B, Xu P, Chang Y, Zhang Y, Wu Y, Zhong W, et al. Biodegradable radiative cooling membrane based on electrospun silk fibroin fiber. *Polym Adv Technol* 2023;34:1716–22.
- [237] Hsu PC, Song AY, Catrysse PB, Liu C, Peng Y, Xie J, et al. Radiative human body cooling by nanoporous polyethylene textile. *Science* 2016;353:1019–23.
- [238] Cai L, Song AY, Li W, Hsu PC, Lin D, Catrysse PB, et al. Spectrally selective nanocomposite textile for outdoor personal cooling. *Adv Mater* 2018;30:1802152.
- [239] Zhang X, Wang W, Shao Z, Li Y, Su Y, Zhang Q, et al. A moisture-wicking passive radiative cooling hierarchical metafabric. *ACS Nano* 2022;16:2188–97.
- [240] Hsu PC, Liu C, Song AY, Zhang Z, Peng Y, Xie J, et al. A dual-mode textile for human body radiative heating and cooling. *Sci Adv* 2017;3:e1700895.
- [241] Liang H, Wang F, Zhang D, Cheng Z, Zhang C, Lin B, et al. Experimental investigation of cost-effective ZnO nanofluid based spectral splitting CPV/T system. *Energy* 2020;194:116913.
- [242] Liang H, Wang B, Su R, Zhang A, Wang F, Shuai Y. A Enhance photoelectric efficiency of PV by optical-thermal management of nanofilm reflector. *Adv Nano Res* 2022;13:475–85.
- [243] Liang H, Su R, Huang W, Cheng Z, Wang F, Huang G. A novel spectral beam splitting photovoltaic/thermal hybrid system based on semi-transparent solar cell with serrated groove structure for co-generation of electricity and high-grade thermal energy. *Energy Convers Manag* 2022;252:115049.
- [244] Sato D, Yamada N. Review of photovoltaic module cooling methods and performance evaluation of the radiative cooling method. *Renew Sustain Energy Rev* 2019;104:151–616.

- [245] Liang H, Wang B, Su R, Zhang Z, Wang F, Shuai Y. Enhance photoelectric efficiency of PV by optical-thermal management of nanofilm reflector. *Adv Nano Res* 2022;13:475–85.
- [246] Zhan Z, Elkabbash M, Li Z, Li X, Zhang J, Rutledge J, et al. Enhancing thermoelectric output power via radiative cooling with nanoporous alumina. *Nano Energy* 2019;65:104060.
- [247] Ahmed S, Li S, Li Z, Xiao G, Ma T. Enhanced radiative cooling of solar cells by integration with heat pipe. *Appl Energy* 2022;308:118363.
- [248] Song WZ, Wang XX, Qiu HJ, Wang N, Yu M, Fan Z, et al. Single electrode piezoelectric nanogenerator for intelligent passive daytime radiative cooling. *Nano Energy* 2021;82:105695.
- [249] Asefi G, Ma T, Wang R. Techno-economic evaluation of photovoltaic thermal system integrated with porous phase change materials: case studies in China. *Energy Convers Manag* 2023;290:117227.
- [250] Khan S, Kim J, Roh K, Park G, Kim W. High power density of radiative-cooled compact thermoelectric generator based on body heat harvesting. *Nano Energy* 2021;87:106180.
- [251] Yu L, Xi Z, Li S, Pang D, Yan H, Chen M. All-day continuous electrical power generator by solar heating and radiative cooling from the sky. *Appl Energy* 2022;322:119403.
- [252] Tian J, Chen L, Qiao R, Xiong K, Zhang W, Miao Y, et al. Photothermal-assist enhanced high-performance self-powered photodetector with bioinspired temperature-autoregulation by passive radiative balance. *Nano Energy* 2021;79:105435.
- [253] Ji Y, Lv S. Experimental and numerical investigation on a radiative cooling driving thermoelectric generator system. *Energy* 2023;268:126734.
- [254] Raman AP, Li W, Fan S. Generating light from darkness. *Joule* 2019;3:2679–86.
- [255] Wang CH, Chen H, Jiang ZY, Zhang XX. Design and experimental validation of an all-day passive thermoelectric system via radiative cooling and greenhouse effects. *Energy* 2023;263:125735.
- [256] Wang CH, Chen H, Jiang ZY, Zhang XX, Wang FQ. Modelling and performance evaluation of a novel passive thermoelectric system based on radiative cooling and solar heating for 24-hour power-generation. *Appl Energy* 2023;331:120425.